This is a post-print (peer-reviewed, corrected) version of Omosanya, K.O., Harishidayat, D., 2019. Seismic geomorphology of Cenozoic slope deposits and deltaic clinoforms in the Great South Basin (GSB) offshore New Zealand. Geo-Marine Letters 39, 77-99. DOI https://doi.org/10.1007/s00367-018-00558-8

Seismic geomorphology of Cenozoic slope deposits and deltaic clinoforms in the Great South Basin (GSB) offshore New Zealand

Omosanya, Kamaldeen Olakunle[1,2,3], Harishidayat, Dicky[3]

[1]Oasis Geoconsulting Limited, Ogun State. Nigeria.
[2]Affiliated Researcher, The Research Centre for Arctic Petroleum Exploration, Norwegian University of Science and Technology, Trondhiem, Norway
[3]Department of Geoscience and Petroleum, Norwegian University of Science and Technology, Trondheim, Norway

Corresponding author: kamaldeen.o.omosanya@ntnu.no (email) & +4797372321 (mobile phone)

Kamaldeen Olakunle Omosanya ORCID: 0000-0001-8959-2329
Dicky Harishidayat ORCID: 0000-0003-3729-2441

Abstract

In this study, the Cenozoic sedimentation and infill history of the Great South Basin (GSB), New Zealand, is analysed from a seismic geomorphologic perspective. A suite of sediment types, including mass-transport deposits (MTDs), deltaic clinoforms, contourite-drifts and turbidites, are documented based on high-quality 3-D seismic reflection data and multiple regional 2-D seismic profiles. The MTDs include older, highly compacted and deeper Paleocene deposits that are markers of late Neogene tectonic reactivation, while the younger MTDs were translated over slopes eroded by drifts. Possible trigger mechanisms for mass wasting may include oversteepened margins, prolonged fluid dissipation and weak geological layers. Sedimentation from the Eocene to Recent was contemporaneous with regional plate reorganisation and syn-orogenic activity. As a result, three distinct Eocene deltaic systems with variably oriented channels and depositional elements provide evidence for changing plate kinematics during the Eocene. The Eocene deltaic systems are river dominated and were deposited during relative rise in sea level under variable flow regimes. The passage of the Antarctic Circumpolar Current in the GSB from the Late Eocene to Oligocene led to the deposition of three elongate, detached contourite drifts. In a final phase of basin infill, hemipelagic sedimentation and deposition by turbidity currents dominated late Neogene sedimentation in the GSB. The analyses presented here demonstrate the importance of geomorphology in understanding the sediment infill history, their interactions and temporal organisation, which have wider implications for numerous geoscience disciplines.

Keywords: Seismic geomorphology, mass-transport deposits, deltaic clinoforms, contourite, turbidites, great south basin

1. Introduction

Seismic geomorphology in the last few decades have revolutionised our understanding of sedimentary processes and has enhanced several related disciplines, such as seismic stratigraphy, paleoenvironment, paleoclimatology and hydrocarbon exploration, in many basins (Zeng et al., 1998; Davies et al., 2004; Posamentier, 2005; Posamentier et al., 2007; Alves et al., 2014). Perhaps the most significant contribution of seismic geomorphology to date is the illumination of the interconnection between sedimentary processes and elements operative in continental to transitional and deep-water environments (Alfaro and Holz, 2014; Bourget et al., 2014). The co-existence of several sedimentary depositional elements during the geodynamic evolution of many basins has been studied in detail using a seismic geomorphologic approach (e.g., Scarselli et al., 2016; Liu et al., 2016).

Seismic geomorphology, in simple terms, is the application of analytical techniques to the study of landforms and ancient geomorphological features imaged by 3-D seismic data (Posamentier et al., 2007). At the heart of such an application lies high-quality three-dimensional (3-D) seismic reflection data, which have led to not only a compendium of sediment types to be identified but also their morphological divisions to be bookmarked. Mass-transport deposits (Ward et al., 2018; Dalla Valle et al., 2013;), contourites (Gong et al., 2017), turbidites and carbonates (Dong et al., 2015; Rankey, 2017), channels and canyons (Harishidayat et al., 2015, Li et al., 2013), gullies (Harishidayat et al., 2018; Lonergan et al., 2013) and other non-sedimentary features (Hillman et al., 2015; Infante and Marfurt, 2017) have been documented using methods of seismic geomorphology. Despite these studies and advances in knowledge, the deepwater remains *terra incognita*, while the study of sedimentary processes remains an interesting topic of research for several geoscience disciplines.

As a result, this study aims at investigating the tectonic control on depositional systems in the study area using a seismic geomorphologic approach. The case study area represents a natural laboratory where several depositional systems are preserved. The Great South Basin (GSB) is a complex intra-continental rift basin located offshore, SE of New Zealand's South Island (Fig. 1a). The GSB formed during the Cretaceous and has several distinct sub-basins containing up to 8 km of sedimentary fill (Anderton, 1982; Cook et al., 1999; Eagles et al., 2004; Grobys et al., 2009; Killops et al., 1997; Lamb, 2011; Uruski, 2010). A secondary objective of this study is to reappraise the hydrocarbon potential of the Great South Basin. This is important considering that the basin has undergone petroleum exploration activity for the last seven decades. Commercial discovery of hydrocarbon remains challenging due to lack of quality data and understanding of the petroleum system, which can be partly attributed to the complex tectonic history of the basin (Cook et al., 1999; Johnston et al., 1996; Uruski, 2010). Hence, this study provides new information on hydrocarbon prospectivity in the GSB. Importantly, the results and techniques presented in this paper have wider industrial and academic implications for understanding sediment interaction with tectonics during the geodynamic evolution of any basin.

2. Regional setting of the Great South Basin

2.1. Geodynamic evolution

The extent of the Great South Basin (GSB) is defined by the 2 km isopach at water depths greater than 300-600 m (Fig. 1a). The geodynamic evolution of the GSB is in three main phases, syn-rift, post-rift and syn-orogenic (Fig. 2; Bache et al., 2014), which are contemporaneous with changes in the regional stress field and relative motion between the Australia, Pacific and Antarctic plates (Fig. 2; Cook et al., 1999; Cox and Sutherland, 2007). The syn-rift phase (112 Ma to 82 Ma) was notably dominated by a horizontal extension (Figs. 2a to 2b). During the Late Cretaceous, rifting involved separation of the Australia, Pacific and Antarctica plates along a complex system of ridges and dispersal of the New Zealand micro-continent within the Pacific plate (Figs. 2a-2b; Bradshaw, 1989; Weaver et al., 1994; Sutherland et al., 2010; Luyendyk, 1995).

The post-rift stage (82 Ma to 19 Ma) phase of basin evolution was dominated by differential subsidence, compaction, tilting and gravitational instabilities (Figs. 2b to 2e). Additionally, the inherited framework of the Late Cretaceous rifting greatly influenced the configuration of the GSB, especially the basement faults, which were active during rifting and are regional crustal structures with a protracted history of activity (Beggs et al., 1990). The basement faults especially influenced selective compressional reactivation during Eocene and Neogene shortening (Figs. 2c to 2e; Bache et al., 2014; Ghisetti, 2010). Furthermore, post-rift sagging was accompanied by strong subsidence in the central part of the basin, localised uplift at previous rift shoulders, and tilting (Bache et al., 2012). Vertical instability during the post-rift stage along the basin's margins likely triggered gravitational soft-sediment deformation and detachments (Bache et al., 2012). This was in addition to horizontal shortening and vertical uplift that were concomitant with the Kermadec subduction (Sutherland et al., 2010; Hackney et al., 2012) and the syn-orogenic stage.

In a final stage of basin development, syn-orogenic tectonics (19 Ma to 0 Ma) involved selective compressional inversion of inherited syn-rift normal faults. This is most evident on the western part of the Great South Basin (Figs. 2d and 2e; Bache et al., 2014; Ghisetti, 2010). Structures developed during this stage have trends compatible with the late Miocene-present stress field and are superposed onto the structures that originated at an earlier stage by tilting and gravitational detachment (Ghisetti, 2010).

2.2. Sedimentary evolution

Cretaceous to Cenozoic sedimentation in the GSB commenced with early basin-fill deposition in small and rifted basins formed during the syn-rift phase at the eastern Gondwana margin (Killops et al., 1997; Cook et al., 1999). Rocks deposited during this period include conglomerate, sandstone, mudstone, and in some places, coal measures of the Hoiho Group (Figs. 2b to 2e). By the Late Cretaceous, widespread fluvial systems that were generally flowing to the northeast had developed along the axes of the major grabens (Killops et al., 1997). With prolonged transgression and continued subsidence in the Late Cretaceous to Paleogene period, the region was gradually drowned in an earlier terrestrial and near-shore

environment (Killops et al., 1997; Uruski, 2010). This transgression climaxed with widespread deposition of organic-rich shales of the Waipawa Formation during the Paleocene-Eocene Thermal Maximum (Nicolo et al., 2007; Killops et al., 2000; Morley et al., 2017).

Rocks deposited during the post-rift phase (Fig. 2) contain terrestrial to shallow marine conglomerate, sandstone and mudstone and minor coal measures (Killops et al., 1997). Fluvio-deltaic systems, including coaly swamps, persisted at the western margin of the GSB while Paleogene turbidites were deposited across the basin floor in front of the delta (Killops et al., 1997). Further transgression during a passive drift phase laid down a thick transgressive marine succession. This succession is approximately 4400 m thick and consists of quartzose sandstone, greensand, and mudstone (Killops et al., 1997). In contrast, deposition in offshore regions was dominated by fine open-water carbonates (Cook et al., 1999). The late Paleogene sediments predominantly were carbonate rocks, as clastic supply to the basin were reduced significantly during this period (Cook et al., 1999).

Rapid uplift and erosion of the Southern Alps and hinterland to the west during the Neogene led to deposition of thin Neogene succession in the Great South Basin (Uruski et al., 2007). This succession consists of mudstone, conglomerate and sandstone (Cook et al., 1999; Killops et al., 1997). On the westernmost part of the GSB, foreset deposition occurred after the Miocene while thin, fine-grained pelagic sediments accumulated in ever deepening waters in the eastern part (Killops et al., 1997). Hence, the modern Great South Basin continental shelf is underlain by a mix of clastic and cold-water carbonate sediments that have prograded across older strata (Cook et al., 1999; Killops et al., 1997).

3. Dataset and research approach

3.1. Dataset

The main seismic data used here are from a Kirchhoff, pre-stack, time-migrated, high-resolution, 3-D seismic reflection dataset (Figs. 1a and 1b) that covers an area of approximately 1345 km^2. The 3-D seismic survey was acquired with eight 6,000 m streamers towed at 10 m to 12 m depths and bin spacing of 12.5 x 12.5 m such that the inlines and crosslines are oriented in the N–S and E–W directions, respectively. In addition to the 3-D data, a 2-D seismic survey called *BO-GSB2D* composed of 25 seismic lines (Fig. 1b) was used to understand the regional geology context of this research and the extent of some of the deposits interpreted here (Fig. 1b). These 2-D lines image down to 8000 ms for two-way travel time (TWTT).

All the seismic data are zero-phase processed and displayed with Society of Exploration Geophysicists (SEG) normal polarity, whereby a downward increase in acoustic impedance is a positive reflection (peak/red reflection) and a downward decrease in acoustic impedance is a negative reflection (trough/blue reflection) on the displayed seismic sections. Well data from the Pakaha-1 wellbore (Figs. 1a, 1b and 3) were used to constrain the lithology and ages of the different horizons and deposits interpreted, as well as average velocities for the Pakaha (2760 m/s), Rakiura (2120 m/s), and overlying

Penrod groups (1400 m/s). Hence, with a dominant frequency of ~50 Hz for the data, the limits of vertical resolution, i.e., λ/4 (Sheriff and Geldart, 1995; Yilmaz, 2001), are approximately 7-11 m and 11-14 m from the Penrod to Rakiura and Pakaha groups, respectively. The horizontal resolution is equal to the bin spacing. For depth conversion of structural maps and units, a time-depth relationship is produced from Pakaha-1 (Fig. 3c).

3.2. Research approach

The approach used here consists of the seismic interpretation of twenty horizons (Figs. 3a and 4), which include the tops of three contourite drifts/deposits (CDs), six horizons marking the limits (i.e., tops and bases) of three deltaic systems and the tops of three mass-transport deposits (MTDs). In addition to seismic interpretation, the variance seismic attribute was used to delineate (a) channels, lobes and fans associated with the deltaic clinoforms, (b) the morphological features within the youngest MTD and (c) polygonal faults and canyons affecting the studied sediments. The variance attribute is a direct measurement of the dissimilarity between seismic traces; it converts a volume of continuity into a volume of discontinuity, highlighting structural and stratigraphic boundaries such as mud volcanoes, salt intrusions, MTDs and polygonal faults (Brown, 2011; Omosanya, 2018). On the variance maps, slightly deformed layers and remnant blocks within the MTD and the polygonal faults are characterised by chaotic reflections with low variance coefficients in contrast to their background values, which have moderate to high variance coefficient reflections. Features identified in the variance time slices were also used as ground truth data for the seismic sections. For example, the channels and canyons on seismic sections are erosional features characterised by onlapping on their margins and by contrasting amplitudes between their fill and adjacent overbank deposits (Gamboa et al., 2012; Harishidayat et al., 2018; Posamentier and Kolla, 2003).

3.3 Interpretation criteria for mass transport deposits, deltaic clinoforms and contourite drifts

Mass-transport deposits in the study area are identified based on seismic description of MTDs as proposed by several previous authors (e.g., Posamentier and Kolla, 2003; Richardson et al., 2011). These include the presence of a top that is usually ridged, rugose or have irregular topographies (Richardson et al., 2011), while the bases are delimited by well-defined basal shear zones or continuous reflections that separate the disrupted strata within the MTD from the much more continuous deposits underneath (Frey-Martínez et al., 2005). Internally, MTDs can include seismically transparent to chaotic seismic reflections depending on the interior architecture derived from their source materials. Hence, most MTDs can comprise slides, slumps and debris flow deposits (Masson et al., 2006), which are geometrically translated as entirely homogeneous, chaotic, and disaggregated material with no original stratigraphy preserved.

The Eocene deltaic systems are characterised based on their internal reflection terminations and configurations such as toplap, downlap, and mounded reflections. Moreover, their evolutionary histories were described using a shoreline trajectory analysis that was applied to shelf-margin clinoforms by Steel

and Olsen (2002). The shoreline trajectory describes the cross-sectional path of the shoreline as it migrates (Helland-Hansen and Gjelberg, 1994; Patruno et al., 2015; Posamentier and Vail, 1988), as a function of bathymetry, sediment supply, eustatic sea-level changes, loading subsidence and compaction (Helland-Hansen and Martinsen, 1996). Clinoform shoreline trajectory may include very low angle-ascending trajectory, a high angle-ascending trajectory, a flat trajectory and a descending trajectory (Johannessen and Steel, 2005). Ascending shoreline trajectories will result in a sigmoidal seismic pattern and long-term rise in the relative base level. Flat and descending trajectories will produce an oblique progradational seismic pattern. A flat trajectory suggests a stable, relative base level through time, usually formed by an optimal sediment supply. A descending trajectory may signify a large sediment supply influenced by relative sea-level fall and strong fluvial input (Helland-Hansen and Martinsen, 1996; Johannessen and Steel, 2005; Helland-Hansen and Hampson, 2009).

Contourite drifts (deposits) are characterised here based on the seismic facies scheme proposed by Rebesco et al. (2014); Rebesco and Stow, (2001); and Stow et al. (2002). These include the observation of parallel or along-slope deposits, mounded elongate geometry, overlying post-drift sediments, underlying pre-drift sediments and an adjacent concave moat. Large-scale cross-stratification and widespread regional discontinuities, especially at the base of the drift are often associated with contourite drifts (e.g., Knutz, 2008; Stow et al., 2013). In addition, a contourite depositional system (CDS) is defined as the association of various drifts and related erosional features (see Hernández-Molina et al., 2003; Rebesco and Stow, 2001; Rebesco and Camerlenghi, 2008).

4. Results and interpretation

4.1 Seismic stratigraphy of the study area

The main sedimentary units intersected by the Pakaha-1 wellbore (Figs. 1 and 3) include the Hoiho (syn-rift), Pakaha (post-rift), Rakiura (post-rift to syn-orogenic), and Penrod (syn-orogenic) groups. Shale of the Wickliffe, Waipama and Laing Formations (Figs. 3a and 3b) dominates the Pakaha Group, while the overlying Rakiura Group include the shale-dominated Laing Formation and the marl-dominated Tucker Cove Formation (Fig. 3). These groups of organic-rich shales were succeeded by deltaic progradation associated with a major Early Eocene lowstand and by contourite deposits in the Middle-Late Eocene (Nicolo et al., 2007; Morley et al., 2017). The regional Marshall Paraconformity marks the Eocene-Oligocene boundary and is bounded at the top and base by contourite deposits and drift sheets (Fulthorpe et al., 1996; Lever, 2007; Uruski and Ilg, 2006). The Penrod Group consists mainly of carbonate sediments from the mid-Oligocene that are younger in age and is characterised by a complex internal structure caused by shelf effects, currents and changing tectonics (Carter and Norris, 1976; Cook et al., 1999; Viskovic, 2011).

Accordingly, horizons H1-H14 are used to describe the stratigraphic framework of the study area (Fig. 3). Horizons H1 to H5 are part of the Palaeocene to Cretaceous interval and are interpreted to understand the structural background of the area prior to the Cenozoic. These horizons belong to the Palaeocene

Wickcliffe Formation and the Cretaceous Hoiho Group (Fig. 3). On seismic sections, from top to base, horizons H1 to H3 specifically delimit chaotic, faulted, low frequency, low to moderate amplitude reflections that were deposited during Cretaceous rifting (Figs. 4-6). In the eastern part of the study area, these sediments and those of the H4-H5 strata generally onlap onto the acoustic basement, which is observed to be granitic in composition from the Pakaha-1 wellbore (Fig. 3a). The Mesozoic history of the Great South Basin are preserved in the basement unit. Above H1-H5, the H5 to H7 strata are characterised by hemipelagic sediments that are continuous, high frequency and moderate to high amplitude reflections on seismic sections (Figs. 3-5).

Furthermore, horizons U1-U6 are interpreted to mark the boundaries of three main Early Eocene deltaic systems (Clinoforms 1-3) between H7 and H8 (Figs. 3-5). These deltaic systems are marked by archetypical sigmoidal to oblique clinoforms on seismic sections (Figs. 3 & 4) and are here interpreted as deltaic clinoforms because they are less than 100 m in vertical relief and greater than 50 km in length (see Patruno et al., 2015). Stratigraphically above Clinoforms 1-3 are hemipelagic and polygonally faulted packages composed of high amplitude, high frequency, and continuous reflections (Figs. 3-6). Polygonal faults are closely spaced normal faults that occur in tiers across the Laing to Tucker Cove Formations (Figs. 3-5). In planform, the polygonal faults have a polygonal outline and include two types, i.e., the northern and southern polygonal fault systems (Fig. 7). Polygonal faults are usually formed by contraction-driven shear failure during the early stages of sediment compaction and dewatering in subsiding sedimentary basins (Goulty, 2001).

Consequently, the upper tips of the polygonal faults reached and are truncated by horizon H11. The sediments underlying H11 are dominantly contouritic sediments and include high frequency, continuous and high amplitude reflections (Figs. 3a-5). Importantly, H11 represents the Eocene-Oligocene boundary or the much-debated regional Marshall Paraconformity in the study area (Uruski and Ilg, 2006; Morley et al., 2017). Here, wide canyons (up to 3.5 to 5 km in width) and turbidite channels forming lateral accretion packages (LAPs) often incise the sediments. In the seismic sections, the reflections making up the Penrod Formation are generally high frequency, continuous, unfaulted and high amplitude except within the canyon or channel fills, which may contain chaotic mixtures of moderate and high amplitude reflections (Figs. 3-5 and 7).

4.2 Interpreted mass-transport deposits (MTD 1-3)

The three main MTDs that are interpreted in the study area are extended beyond the 3-D seismic data; they include Palaeocene MTD 1 and 2, and Oligocene-Recent MTD 3 (Figs. 1b, 3-6). MTD 1 is oriented in a NW-SE direction and covers an area of approximately 6,058 km^2 with an estimated average run out distance of approximately 109 km (Fig. 1b and Table 1). MTD 1 contains variable packages that include chaotic reflections (debris flow deposits) at the base to slightly deformed layers (slumps) at the top (Figs. 3-6). In the northern part of the study area, chaotic to strongly deformed reflections (slumps) dominantly underlie MTD 1 (Fig. 6b). Additionally, several seismic high amplitude anomalies that are indicative of fluid in the subsurface are observed to be associated with MTD 1 (Figs. 4, 6a and 6b). These anomalies

are characterised by reverse polarities in comparison to the seafloor reflection or signal (See Alves et al., 2014). In addition to the fluid anomalies, the base of MTD 1 is regularly intersected by faults, some of which are related to the extension of the underlying Hoiho Group (Figs. 3 and 4), while others indicate regional reactivation of faults during the Cenozoic in the study area (e.g., Figs. 5 and 6).

Estimated area coverage and average run out distance of MTD 2 are approximately 4,074 km^2 and 88 km, respectively (Figs. 1b and Table 1). MTD 2 trend in the N-S direction with its headwall domain inferred to the northern part of the study area, where elevated topographies underlying horst fault blocks are observed (Fig. 1b). On seismic sections, MTD 2 also contains chaotic reflections (debris flow deposits) at the base and slightly deformed layers (slumps) towards the top (Figs. 3-6). Neither faults nor fluid anomalies are associated internally with MTD 2, which contrasts with MTD 1, which is severely faulted. Although not significantly faulted, MTD 2 is mildly deformed by late tectonic activities with some fault-related folds or monoclines observed internally in the MTD towards to the eastern part of the study area (e.g., Figs. 5 and 6b).

MTD 3 is Oligocene-Recent in age and is oriented in a W-E direction with an approximate area coverage of 855 km^2 and run out distance of 51 km (Figs. 1b and Table 1). Unlike the two older MTDs, MTD 3 shows some morphologic features commonly found within MTDs. This includes the presence of a discernible headwall domain located in the western part of the 3-D survey where contourite mounds predominate (Figs. 1b and 7). In addition, remnant blocks that are positioned at the upper tips of polygonal faults are also interpreted within MTD 3 (Figs. 7 and 8). Remnant blocks are in situ elements of mass-transport deposits that were not removed by erosion, and they usually show vertical stratigraphic continuity with underlying non-MTD strata, lacking a gliding surface (Alves, 2015; Ward et al., 2018). On the variance time slice, the remnant blocks are marked by areas of a very low variance coefficient relative to areas of chaotic-moderate variance coefficients associated with the rest of MTD 3. Heights of remnant blocks with MTD 3 can reach up to 140 m (e.g., Figs. 8a and 8b).

The ridged topographies of the top MTD 3 unit is often associated with some erosional features that are here interpreted as channels (Fig. 8a). Specifically, in the western part of MTD 3, a large canyon system that is approximately 6 km wide incised the top MTD horizon (Figs. 7 and 8b). These channels and canyons show lateral migration, internal fill that varies from high amplitude at the base to chaotic reflection at their tops, cut and fill character, and vertical stacking (Fig. 3 and 8). These characteristics are typical of channels and canyons that are dominated by a turbidity current (See Reading and Richards, 1994; Mayall et al., 2006; 2010). Additionally, MTD 3 is delimited in its northern and southern parts by two different polygonal fault systems (Fig. 7), which are rooted in the underlying Laing Formation (Figs. 3 and 7).

4.3 Eocene deltaic clinoforms

Three main kinds of clinoforms were recognized in the study area (Figs. 9 to 11). These include prograding sigmoid clinoforms in Clinoform 1 (Figs. 4, 9a and 9b), prograding and complex sigmoid to

oblique clinoforms in Clinoform 2 (Figs. 4, 5, 10a and 10b) and prograding parallel to sigmoid clinoforms in Clinoform 3 (Figs. 4, 11a and 11b). Prograding sigmoid clinoforms consists of nearly S-shaped reflections with thin, gently dipping upper and lower segments, and thicker, more steeply dipping middle segments (Figs. 4, 5, 9 to 11). The upper segments form the topset, which is concordant with the overlying reflections, while the thicker middle segments (i.e., the foresets) are inclined and connect the topset to the bottomset. The bottomset (lower segments) is almost parallel to the underlying reflections. Hence, the general configuration of prograding sigmoid clinoforms shows laterally displaced strata in a depositional downdip direction (outbuilding or progradational patterns). In oblique clinoforms, the foreset strata downlap on an underlying surface meanwhile the topset is absent and the foresets terminate upward against a toplap surface or truncation (Figs. 4, 11a and 11b).

Subsequently, the direction of transport for the deltaic sediments was determined from the combined thickness of the clinothems (Fig. 12). Each deltaic system demonstrates unique depositional trends and several interpreted clinothems i.e., the sedimentary packages bounded by these clinoforms. The number of clinothems are 12, 6, and 4 from Clinoforms 1 to 3 (Figs. 9-11), with the sediments of Clinoform 1 generally thickening towards the northeastern and southern part of the study area, whilst Clinoforms 2 and 3 thicken towards the SE part (Figs. 12a-12c). Thus, the isopach maps indicate a general NW-SE direction of transport for Clinoforms 1 to 3 (Fig. 12d). In addition to the depositional trends, the morphologic positioning of topset, foreset and bottomset for the clinoforms are manifested on the isopach maps (Fig. 12).

In support the inferred direction of transport and interpreted clinoform configurations, the shoreline trajectory analyses show that Clinoforms 1 and 2 clinoforms are dominated by descending - ascending to regressive clinoforms, while Clinoform 3 has an ascending-descending trajectory (Figs. 9c, 10c, and 11c), an indication that the development of Clinoforms 1 and 2 was accompanied by the extension of its distributary channels and mouth-bars towards the southeastern part of the study area, while the channels and mouth-bar system of Clinoform 3 are in the NE direction (Figs. 13 and 14). This interpretation is supported further by several NW-SE oriented channels that are interpreted at the base of Clinoforms 1 and 2 (Figs. 13a, 13b and 14).

On the variance time slices, wide lobes or fans that are more than 8 to 15 km in width are interpreted to be associated with these channels. These lobes/fans are reflected as areas of moderate variance coefficients adjoining areas of very low variance coefficients and linear features, i.e., the channels (Fig. 13). Five lobes that are oriented in the NE, E and SE directions are associated with Clinoform 1 (Fig. 13a), while one fan is associated with Clinoform 2 (Fig. 13b). The channels interpreted at the base of Clinoform 3 show more N to NE orientations relative to an inferred lobe, which is oriented to the east (Fig. 13c). Based on this seismic evidence and interpretation, the Eocene deltaic systems in the study area are categorised as river-dominated deltas (sensu Bhattacharya, 2006; Galloway, 1975; Walker, 1992). River-dominated deltas are characteristically elongate to lobate in geometry and are associated

with straight to sinuous distributary channels mouth bars such as those interpreted in Figs. 13 and 14 (see also Galloway, 1975).

4.4 Interpreted contourite depositional system (CDS)

In the study area, a *contourite depositional system* is interpreted within the uppermost Laing Formation. The CDS contains three elongate contourite drifts with tops that correspond to horizons H8-H10 (Fig. 15). All the drifts are elongate in the N-S direction and located in the proximal north western part of the study area outside the 3-D seismic survey (Fig. 15). In fact, the mounds were interpreted on the regional 2-D lines, while bends that are associated with two of the drifts were observed from the 3-D survey. These bends or areas of marked change in slope gradients (Figs. 15 and 16) are interpreted as deviations in the paths of the contour currents that produced the drifts (see Faugères et al., 1999). Chronologically, the horizons from H8 to H10 correspond to the upper parts of the Laing Formation and the top of the Tucker Cove Formation. Hence, the oldest mound is dated from the Mid Eocene to Late Eocene, while the last two mounds are possibly Late Eocene to Oligocene in age (Figs. 3, 15 and 16).

In terms of morphometry, the oldest drift (H8) covers an area of approximately 1540 km^2 with a length of approximately 172 km (Figs. 15b and 15c, Table 1). The height of the drift is approximately 1.19 km (Table 1) and has an associated bend that is approximately 52.4 km long and 21 km wide (Figs. 15c and 16). Characteristically on seismic sections, the oldest mound caps several SW to NE gently dipping cross stratifications (Figs. 15a and 15b). Furthermore, the second drift (H9) is interpreted above very continuous and high amplitude reflections where no cross stratification is observed (Figs. 15a and 16). The area coverage, length and height of this drift on H9 are 1540 km^2, 172 km and 1.16 km, respectively (Table 1). In contrast, the youngest drift (H10) covers an area of approximately 2177 km^2 and 202.4 km long with an estimated height of 1.17 km (Table 1). This drift is also associated with bi-directional cross stratifications on seismic sections (Figs. 15 and 16) and a bend that is approximately 78 km long and 55 km wide. In addition to all these features, younger MTDs apart from the one discussed in section 3.1, and channels are observed above this drift (Figs 15a and 15b).

In addition to their geometries, it is important to describe the drifts in terms of their flow direction and currents. Bottom current flow direction and drift migration are inferred from the internal reflection progradation as contourite drifts can often migrate along the slope and down current (e.g., Faugères et al., 1999). The recognition of along slope prograding internal reflections within contourite drifts is an important marker of the depositional current flow direction (e.g., Knutz and Cartwright, 2004). Figs. 15 and 16 shows that the drifts are oriented essentially in the N-S direction, which is suggestive of the action of N-S oriented bottom currents in the Great South Basin during this interval. Additionally, the structural maps at the mounds' top show an eastward migration of the drifts from the Mid Eocene to Oligocene period. The presence of erosional features or bends on one side of these mounds show that they are likely separated, elongated, mounded drifts. Such drifts are usually found on a steeper, lower slope (Rebesco and Stow, 2001; Stow et al. 2002). The associated bends in turn are mostly erosional and non-depositional, representing an area where the flow was focused and diverted.

5. Discussion

5.1 Cenozoic sedimentation and evolution of the Great South Basin

The Cenozoic infill history of the basin is revealed by temporal and spatial stratigraphic organisation of distinctive sediment types, which reflects the complex interaction of many depositional processes and conditions. The Wickliffe Formation marks the Cretaceous-Palaeocene boundary and was deposited on topographies or basin architectures developed during the transition from the Gondwana subduction to extension. Although the formation is predominantly transgressive in nature (Cook et al., 1999; Killops et al., 1997), two Palaeocene MTDs are observed here that are possibly triggered by a combination of a steepened basin margin and protracted fluid dissipation. Both MTDs are part of the post rift sediments and are underlain by several magmatic sills on the regional 2-D lines (Fig. 1b). These sills are likely related to break-up magmatism in the Cretaceous period. Hence, we considered magmatic fluids and weakened geologic layers because of prolonged fluid dissipation as possible trigger mechanisms that reduced the shear strength of the paleo seafloor sediments and resistance to slope failure. More so, the headwall region of MTD 1 and 2 are inferred in elevated margins to the west. These elevated margins correspond to the location of horsts and other fault-related basement highs produced during rifting in the western part of the GSB. Although MTD 1 and 2 are severely faulted in the western and northern part of the study area, these latter faults are imprints of younger tectonic reactivation and syn-orogenic activities later in the Neogene.

Late Palaeocene to Early Eocene sedimentation was dominated by hemipelagic deposition (Figs. 3-6), with most detritus sourced from subaerial erosion of the Eastern Gondwana (Bache et al., 2014). Marine transgression in the Palaeocene was followed by shallowing to coastal environments as indicated by the Eocene clinoforms. Eocene deltaic systems are essentially fluvial-dominated and deposited during long-term relative sea level still stands (Figs. 9-13). Importantly, Eocene and subsequent sedimentation was associated with tectonic reorganisation and development of the modern Australia–Pacific plate boundary, including the Tonga–Kermadec subduction system (Bache et al., 2012, 2014). After the deposition of the prograding Eocene deltaic sediments, the study area returned to a marine setting with deposition of younger hemipelagic sediments. Notably, the Antarctic Circumpolar Current (Kennett et al., 1975; Fulthorpe et al., 1996) actively eroded the upper slope and shelf area, leading to the formation of elongate contourite drifts (Figs. 15 and 16).

As contourites can also indicate variability in paleo-current and paleo-climatic regimes (Rebesco et al., 2014; Knutz, 2008; Hernández-Molina et al., 2014). The regional Marshall Paraconformity (H11) in the study area and its associated drifts provide indications of paleo-climatic conditions of the Great South Basin from the Middle Eocene to Oligocene. The Marshall unconformity is related to the onset of the Antarctic Circumpolar Current (ACC), which is a key feature of the Southern Ocean (Kennett et al., 1975; Fulthorpe et al., 1996). The ACC helped cool Antarctica and initiate Southern Hemisphere glaciation. Hence, it was associated with global change from an ocean with warm saline deep water

formed at low latitudes and dominated by halothermal circulation to a thermohaline system with cold deep water that was formed at high latitudes (Kennett and Stott, 1990; Fulthorpe et al., 1996; Lyle et al., 2007). Although the present orientation of the drifts and their inferred current directions might not necessarily correspond to the East-West orientation of the ACC, it is important to stress that the trend observed here for the drifts might represent localised fluctuation in the ACC flow. This is especially valid considering that the GSB was tectonically active during the Middle Eocene to Oligocene interval.

Post-Oligocene, overloading of the hemipelagic sediments presumably led to the formation of two different tiers of polygonal faults in the lower slope areas, (Fig. 7). The accurate timing of these polygonal fault tiers remains ambiguous (Morley et al., 2017). Recent sedimentation includes the deposition of several discrete MTDs atop the contourite drifts, additional hemipelagic sedimentation and erosion of the substrate by large-scale turbidite channels (Figs. 3, 8 and 15). Among the younger MTDs is MTD 3, which is composed of large remnant blocks, an indication that MTD 3 is proximal to the source area. Possible trigger mechanisms for MTD 3 include subsurface fluid dissipation from the polygonal faults (Fig. 8), erosion of the substrate by bottom currents and the presence of weak geological layers, i.e., the hemipelagic sediments (Figs. 15 and 16). The development of polygonal faults is intimately tied to compaction-related dewatering, which represents a ubiquitous process for fluid release in many basins (Dewhurst et al., 1999). Hence, fluids expelled from the polygonal systems are capable of aiding slope failure and translation of MTD 3 and younger MTDs on top of the drifts.

5.2 Dynamic evolution of the Eocene deltaic systems

Toplap terminations of both Clinoforms 1 and 2 signify non-deposition (sedimentary bypass) and only minor erosion at their depositional boundaries (Mitchum Jr et al., 1977). In addition, the sigmoid and mounded internal configuration of Clinoform 1 particularly reflects relatively low sediment supply, rapid basin subsidence, and/or rapid relative sea level rise to allow deposition and preservation of the topset units (Mitchum Jr et al., 1977; Sangree and Widmier, 1977), an indication of a relatively low-energy regime. Most of these depositional conditions are also true for clinoforms within Clinoform 2. However, the complex sigmoid-oblique configuration of Clinoform 2 indicates a history of alternating upbuilding and depositional bypass in the topset segment within a high-energy depositional regime (Mitchum Jr et al., 1977). Furthermore, the parallel – sigmoid configuration (early stage and last stage development of Clinoform 3, respectively) of Clinoform 3 indicates some combination of relatively high to low sediment supply, slow to rapid basin subsidence, and a stillstand to rapid rise in sea level (Mitchum Jr et al., 1977).

The shoreline trajectories for both Clinoforms 1 and 2 indicate a combination of descending - ascending regressive shorelines trajectories. Hence, sands have higher potential to accumulate on the topset and foreset rather than on the bottomset of the deltaic clinoform system (Helland-Hansen and Hampson, 2009). Additionally, ascending trajectories could also result in a sigmoidal seismic pattern and a long-term rise in relative sea-level (see Helland-Hansen and Martinsen, 1996). Thus, long-term rising of relative sea-level generated accommodation behind the shorelines, providing space for net aggradation of non-marine and/or transition deposits (Figs. 14a and 14b), which allowed the associated distributary

channels and mouth-bar system to move distally in a SE direction (Figs. 13a and 13b; Helland-Hansen and Gjelberg, 1994; Helland-Hansen and Martinsen, 1996). Although Clinoform 1 shows potential for more accommodation space seaward than Clinoform 2 (Fig. 12), this is most apparent from the isopach maps where the area covered by the foreset and bottomset beds of Clinoform 1 are larger than in Clinoform 2 (Fig. 12). Nonetheless, both clinoforms show characteristics of distributary channels that may cause the mouth bar and channel to form elongate bar-finger sands (*cf.* Bhattacharya, 2006; Fisk, 1961).

Relative to Clinoform 1 and 2, Clinoform 3 (Fig. 12) is located landward and characterised by complex parallel-sigmoid clinoforms within Clinoform 3, which signal uniform rates of deposition on a uniformly subsiding shelf or stable basin plain setting, which allowed the deposition and preservation of the topset (Mitchum Jr et al., 1977; Sangree and Widmier, 1977). In addition, the descending regressive - accretionary trajectory of Clinoform 3 (Figs. 11c and 14c) may signify a large sediment supply that was influenced by a strong fluvial input during a relative short period of sea-level fall (Helland-Hansen and Hampson, 2009; Helland-Hansen and Martinsen, 1996). These conditions may account for the spatial development of a deltaic system that shifted in the northeast direction and development of a foreset area that is wider towards the northeastern part of the study area (Fig. 12c and 13c). As a corollary, sediments (clinothems) within Clinoform 3 are likely deposited under a different flow regime when sediment bypasses the older deltaic system below to deposit a new (but smaller) deltaic system further east (Fig. 13c; see Bates, 1953; Bhattacharya, 2006; Mulder et al., 2003; Mulder and Alexander, 2001; Mulder and Chapron, 2011; Zavala et al., 2011).

In addition to the depositional conditions that were prevalent during the Eocene, it is possible that the variation in the orientation of the different distributary channels and mouth bars may reflect the influence of nearshore currents such as waves, tides or sediment dynamics during the Eocene geodynamic evolution of the Great South Basin. Waves and tides can generate the larger stretches of the shoreline recorded, especially during the deposition of Clinoform 3 (Fig. 14c). Tide- and wave-influenced shorelines can typically have wider shelves and large embayment such as the northern Australia coast (Vakarelov et al., 2012). However, the role of regional plate kinematics on the orientation of the interpreted distributary channels and mouth bars is significant since the Late Eocene marks a transition from seafloor spreading between New Zealand and Gondwana to the emergence of the Tonga–Kermadec subduction from approximately 50 Ma (Fig. 2). More so, Eocene to Recent sedimentation in the GSB was associated with regional plate re-organisation (Bache et al., 2012, 2014). Hence, the change in orientation of the channels and mouth bars were from dominant NW-SE orientations in Clinoforms 1 and 2 to E-W and NE-SW orientations for Clinoform 3 (Figs. 13 and 14d). Therefore, the clinoforms and their associated depositional elements are considered as markers of plate dynamics in the GSB.

5.3 Implications for hydrocarbon prospectivity in the GSB

5.3.1 Mass-transport deposits

Apart from MTD 3 and the younger MTDs on the flanking positions of the drifts, the deeper MTD 1 and 2 are in the class of older and deeper MTDs described from many basins, which usually have their initial stratigraphy and geomorphologic features unpreserved due to compaction and deep burial. Hence, MTD 1 and 2 are comparable in their internal structure to their confining strata (see Ogiesoba and Hammes, 2012). Importantly, the chaotic reflections (Figs. 3 and 4) and slightly deformed layers (Fig. 6) within both MTDs imply that they are mud prone and comprise relatively poor reservoir units (Posamentier and Kolla, 2003; Jennette et al., 2000). On the other hand, the undeformed blocks in MTD 3 show high amplitude strata, theoretically an indication of sand prone reservoir targets (see also Omosanya and Alves, 2013; Alves, 2015). As seal rocks, the observation of several bright spots or amplitude anomalies below MTD 1 and 2 shows that they have potentially trapped fluids and are low permeability seal rocks (Figs. 4 and 6).

5.3.2 Eocene Deltaic systems

Since the Eocene deltaic system in the study area are interpreted to be the product of a long-term relative sea-level rise produced by variable flow regimes. The associated deposits are therefore proposed to be composed essentially of mud (Bhattacharya, 2006; Bhattacharya and Walker, 1992; Shanley and McCabe, 1994). These mud-rich systems are candidate source rocks in the study area where the development of stratified water columns and physio-geographic restriction can increase the chances of anoxic conditions and organic-rich facies during a long-term sea-level rise (sensu Myers, 2009). Additionally, the high amplitude and isolated seismic reflections (Figs. 9-11) that are associated with Clinoforms 1 to 3 are interpreted to be sand-rich distributary channel-fill (sensu Deptuck et al., 2003; Harishidayat et al., 2015; Mayall et al., 2006; Patruno et al., 2015). In Clinoforms 1 and 2, the distribution and areal extent of these sand-prone deposits/channel fills are much higher and can have widths that vary from 100-800 m. These fills here are not vertically stacked but laterally distributed as prograding packages that are bounded by flooding surfaces (Figs. 9-11).

5.3.3 Contourite depositional system (CDS)

One striking importance of contourite drifts observed in the study area is their ability to promote mass wasting in the deepwater environment (Figs. 7, 15 and 16). Contourite drifts generally favour the formation of pressurised gliding planes for slope failure because they usually contain gravitationally unstable and fine-grained deposits with low permeability and high-pore water content (Rebesco et al 2014, Bryn et al., 2005; Solheim et al., 2005; Laberg et al., 2005; Omosanya, 2018). As a proof of this characteristic, the recent mass-transport deposits here are triggered on inclined margins of the mounds where unconsolidated hemipelagic sediments predominate (e.g., Figs. 8 and 16). Furthermore, contour currents can affect the petroleum system in numerous ways by creating sealing rocks and reworking texturally immature reservoir sands (Shanmugam, 2006; Mutti and Carminatti, 2012). Drifts with bi-directional stratifications such as in Figs. 16a and 16b may represent sandy contourite end members

provided that the sands are preserved on the foreset of the clinoforms. In parallel, the overlying high amplitude reflections between H8 and H9 (Fig. 16a) may represent shale or sealing rocks for the sands.

6. Conclusions

This study has investigated the types and dynamics of sediments deposited in the Great South Basin during the Cenozoic using seismic reflection datasets and a seismic geomorphologic approach. The interpretation presented here are solely based on the seismic facies and geomorphology of the different depositional elements. Hence, it has the same downside as most seismic features in that the sediments described here are not actually drilled and their lithology could not be authenticated. Nonetheless, the main conclusions from this study are as follows:

- The Cenozoic basin infill history of the Great South Basin is influenced by the interplay of several depositional elements and processes. Gravity-driven processes, foreset progradation and activities of bottom currents dominate sedimentation in the area over a rifted and complex topography. These sedimentation processes are intermixed with variation in plate kinematics during the Early Eocene. As a result, the Great South Basin records a unique succession of sedimentary deposits deposited by variable flow regimes under different tectonic conditions.
- The three main MTDs in the study are two Palaeocene deposits that are likely triggered by oversteepened margins linked to Cretaceous-Paleocene fault blocks on the western part of the basin and fluids associated with break-up magmatism. The younger MTD 3 shows a propensity towards upward migrating compaction-driven fluids released from polygonal fault systems and slope instability on the margins of contourite mounds. In terms of petroleum systems, the older MTDs have the potential to trap fluids and act as seal rocks as they appear to be highly compacted, while MTD 3 is probably sand-prone and a good reservoir rock considering that it is composed of remnant and less disaggregated blocks.
- Early Eocene deltaic systems are mainly river-dominated and defined by prograding sigmoid clinoforms in Clinoform 1, prograding and complex sigmoid to oblique clinoforms in Clinoform 2 and prograding parallel to sigmoid clinoforms in Clinoform 3. Their associated depositional elements such as channels, mouth bars and lobes are oriented differently from Clinoforms 1-3 suggesting changes in sediment transport direction in relations to plate movements during the Tonga–Kermadec subduction.
- Contourite drifts are parallel or along-slope deposits with mounded elongate geometry and were formed by the Antarctic Circumpolar Current formed in the study area when the global climate changed from low latitudes to high latitudes during the Eocene-Oligocene. Drifts capping bi-directional cross-

stratification represent possible end-member sand-prone systems, while other drifts may be seal units or source rocks for hydrocarbon.

- Above the contourites are high amplitude and high frequency hemipelagic deposits, which are incised by channels and canyons at the uppermost stratigraphic interval. The lateral migration, internal configuration, cut and fill character and vertical stacking of the channels and canyons show that they are formed by turbidity currents.

Acknowledgements

The seismic and well data used here were made available by the New Zealand Government through New Zealand Petroleum and Minerals (www.nzpam.govt.nz) as part of the *exploration data pack*. Schlumberger is gratefully acknowledged for the provision of Petrel® for seismic interpretation at the Department of Geoscience and Petroleum, Norwegian University of Science and Technology, NTNU. We are indebted to the journal editor and reviewers for their contributions and insightful suggestions during the review process.

References

Alfaro, E., Holz, M., 2014. Seismic geomorphological analysis of deepwater gravity-driven deposits on a slope system of the southern Colombian Caribbean margin. Marine and Petroleum Geology 57, 294-311.

Alves, T.M., Kurtev, K., Moore, G.F., Strasser, M., 2014. Assessing the internal character, reservoir potential, and seal competence of mass-transport deposits using seismic texture: A geophysical and petrophysical approach. AAPG bulletin 98, 793-824.

Alves, T.M., 2015. Submarine slide blocks and associated soft-sediment deformation in deep-water basins: A review. Marine and Petroleum Geology 67, 262-285.

Anderton, P., 1982. Great South and Campbell basins, New Zealand: Evaluation of geology and hydrocarbon potential, Far East Rep. 828, Phillips Pet. Co., Singapore.

Bache, F., Mortimer, N., Sutherland, R., Collot, J., Rouillard, P., Stagpoole, V., Nicol, A., 2014. Seismic stratigraphic record of transition from Mesozoic subduction to continental breakup in the Zealandia sector of eastern Gondwana. Gondwana Research 26, 1060-1078.

Bache, F., Sutherland, R., Stagpoole, V., Herzer, R., Collot, J., Rouillard, P., 2012. Stratigraphy of the southern Norfolk Ridge and the Reinga Basin: A record of initiation of Tonga–Kermadec–Northland subduction in the southwest Pacific. Earth and Planetary Science Letters 321-322, 41-53.

Bates, C.C., 1953. Rational theory of delta formation. AAPG Bulletin 37, 2119-2162.

Beggs, J.M., Challis, G.A., Cook, R.A., 1990. Basement geology of the Campbell Plateau: Implications for correlation of the Campbell Magnetic Anomaly System. New Zealand Journal of Geology and Geophysics 33, 401-404.

Bhattacharya, J.P., 2006. Deltas, in: Posamentier, H.W., Walker, R.G. (Eds.), Facies Models Revisited. SEPM SP84, Tulsa, Oklahoma, USA, p. 237.

Bhattacharya, J.P., Walker, R.G., 1992. Deltas, in: Walker, R.G., James, N.P. (Eds.), Facies Models: Response to Sea Level Change. Geological Association of Canada, Canada, pp. 157 - 177.

Bourget, J., Ainsworth, R.B., Thompson, S., 2014. Seismic stratigraphy and geomorphology of a tide or wave dominated shelf-edge delta (NW Australia): Process-based classification from 3D seismic attributes and implications for the prediction of deep-water sands. Marine and Petroleum Geology 57, 359-384.

Bradshaw, J.D., 1989. Cretaceous geotectonic patterns in the New Zealand Region. Tectonics 8, 803-820.

Brown, A., 2011. Interpretation of Three-Dimensional Seismic Data. AAPG and SEG.

Bryn, P., Berg, K., Stoker, M.S., Haflidason, H., Solheim, A., 2005. Contourites and their relevance for mass wasting along the Mid-Norwegian Margin. Marine and Petroleum Geology 22, 85–96.

Cartwright, J., Huuse, M., 2005. 3D seismic technology: the geological *Hubble*. Basin Research 17, 1-20.

Carter, R.M., Norris, R.J., 1976. Cainozoic history of southern New Zealand: An accord between geological observations and plate-tectonic predictions. Earth and Planetary Science Letters 31, 85-94.

Cook, R.A., Sutherland, R., Zhu, H., 1999. Cretaceous-Cenozoic geology and petroleum systems of the Great South Basin, New Zealand. Institute of Geological & Nuclear Sciences.

Cox, S.C., Sutherland, R., 2007. Regional Geological Framework of South Island, New Zealand, and its Significance for Understanding the Active Plate Boundary, in: Okaya, D., Stern, T.A., Davey, F.J. (Eds.), A Continental Plate Boundary: Tectonics at South Island, New Zealand. American Geophysical Union, Washington DC.

Dalla Valle, G., Gamberi, F., Rocchini, P., Minisini, D., Errera, A., Baglioni, L., Trincardi, F., 2013. 3D seismic geomorphology of mass transport complexes in a foredeep basin: Examples from the Pleistocene of the Central Adriatic Basin (Mediterranean Sea). Sedimentary Geology 294, 127-141.

Davies, R.J., Stewart, S.A., Cartwright, J.A., Lappin, M., Johnston, R., Fraser, S.I., Brown, A.R., 2004. 3D Seismic Technology: Are We Realising Its Full Potential? Geological Society, London, Memoirs 29, 1-10.

Deptuck, M.E., Steffens, G.S., Barton, M., Pirmez, C., 2003. Architecture and evolution of upper fan channel-belts on the Niger Delta slope and in the Arabian Sea. Marine and Petroleum Geology 20, 649-676.

Dewhurst, D.N., Cartwright, J.A., Lonergan, L., 1999. The development of polygonal fault systems by syneresis of colloidal sediments. Mar. Pet. Geol. 16, 793–810.

Dong, Y., Zhu, X., Xian, B., Hu, T., Geng, X., Liao, J., Luo, Q., 2015. Seismic geomorphology study of the Paleogene Hetaoyuan Formation, central-south Biyang Sag, Nanxiang Basin, China. Marine and Petroleum Geology 64, 104-124.

Eagles, G., Gohl, K., Larter, R.D., 2004. High-resolution animated tectonic reconstruction of the South Pacific and West Antarctic Margin. Geochemistry, Geophysics, Geosystems 5.

Faugères, J.-C., Stow, D.A.V., Imbert, P., Viana, A.R., 1999. Seismic features diagnostic of contourite drifts. Marine Geology 162, 1–38.

Fisk, H.N., 1961. Bar-finger sands of Mississippi delta. AAPG Special Volume 22: Geometry of sandstone bodies.

Frey Martinez, J., Cartwright, J., Hall, B., 2005. 3D seismic interpretation of slump complexes: examples from the continental margin of Israel. Basin Research 17, 83-108.

Fulthorpe, C.S., Carter, R.M., Miller, K.G., Wilson, J., 1996. Marshall Paraconformity: a mid-Oligocene record of inception of the Antarctic circumpolar current and coeval glacio-eustatic lowstand? Marine and Petroleum Geology 13, 61-77.

Galloway, W.E., 1975. Process framework for describing the morphologic and stratigraphic evolution of deltaic depositional systems. Houston Geological Society Bulletin Deltas: Models for exploration 87-98.

Gamboa, D., Alves, T.M., Cartwright, J., 2012. A submarine channel confluence classification for topographically confined slopes. Marine and Petroleum Geology 35, 176-189.

Ghisetti, F. 2010. Structural Analysis of the Great South Basin in *Seismic Interpretation, Prospects and Structural Analysis, Great South Basin*, Ministry of Economic Development New Zealand Unpublished Petroleum Report PR4173.

Gong, C., Peakall, J., Wang, Y., Wells, M.G., Xu, J., 2017. Flow processes and sedimentation in contourite channels on the northwestern South China Sea margin: A joint 3D seismic and oceanographic perspective. Marine Geology 393, 176-193.

Goulty, N.R., 2001. Polygonal fault networks in fine-grained sediments – an alternative to the syneresis mechanism. First Break 19, 69-73.

Grobys, J.W.G., Gohl, K., Uenzelmann-Neben, G., Davy, B., Barker, D., 2009. Extensional and magmatic nature of the Campbell Plateau and Great South Basin from deep crustal studies. Tectonophysics 472, 213-225.

Hackney, R., Sutherland, R., Collot, J., 2012. Rifting and subduction initiation history of the New Caledonia Trough, southwest Pacific, constrained by process-oriented gravity models. Geophysical Journal International 189, 1293-1305.

Harishidayat, D., Omosanya, K.d.O., Johansen, S.E., 2015. 3D seismic interpretation of the depositional morphology of the Middle to Late Triassic fluvial system in Eastern Hammerfest Basin, Barents Sea. Marine and Petroleum Geology 68, Part A, 470-479.

Harishidayat, D., Omosanya, K.O., Johansen, S.E., Eruteya, O.E., Niyazi, Y., 2018. Morphometric analysis of sediment conduits on a bathymetric high: Implications for palaeoenvironment and hydrocarbon prospectivity. Basin Research doi:10.1111/bre.12291.

Helland-Hansen, W., Gjelberg, J.G., 1994. Conceptual basis and variability in sequence stratigraphy: a different perspective. Sedimentary Geology 92, 31-52.

Helland-Hansen, W., Hampson, G.J., 2009. Trajectory analysis: concepts and applications. Basin Research 21, 454-483.

Helland-Hansen, W., Martinsen, O., 1996. Shoreline trajectories and sequences; description of variable depositional-dip scenarios. Journal of Sedimentary Research 66, 670-688.

Hernández-Molina, F.J., Llave, E., Preu, B., Ercilla, G., Fontan, A., Bruno,M., Serra, N., Gomiz, J.J., Brackenridge, R.E., Sierro, F.J., Stow, D.A.V., García,M., Juan, C., Sandoval, N., Arnaiz, A., 2014. Contourite processes associated to the Mediterranean Outflow Water after its exit from the Gibraltar Strait: global and conceptual implications. Geology 42, 227–230.

Hernández-Molina, J., Llave, E.a., Somoza, L., Fernández-Puga, M.C., Maestro, A., León, R., Medialdea, T., Barnolas, A., García, M., del Río, V.c.D.a., 2003. Looking for clues to paleoceanographic imprints: a diagnosis of the Gulf of Cadiz contourite depositional systems. Geology 31, 19-22.

Hillman, J.I.T., Gorman, A.R., Pecher, I.A., 2015. Geostatistical analysis of seafloor depressions on the southeast margin of New Zealand's South Island — Investigating the impact of dynamic near seafloor processes on geomorphology. Marine Geology 360, 70-83.

Infante-Paez, L., Marfurt, K.J., 2017. Seismic expression and geomorphology of igneous bodies: A Taranaki Basin, New Zealand, case study. Interpretation 5, SK121-SK140.

Jennette, D.C., Garfield, T.R., Mohrig, D.C., Cayley, G.T., 2000. The interaction of shelf accommodation, sediment supply and sealevel in controlling the facies, architecture and sequence stacking patterns of the Tay and Forties/Sele basin-floor fans, Central North Sea. In: Weimer, P., Slatt, R.M., Coleman, J., Rosen, N.C., Nelson, H., Bouma, A.H., Styzen, M.J., Lawrence, D.T. (Eds.), Deep-water Reservoirs of the World: Gulf Coast Society of the Society of Economic Paleontologists and Mineralogists Foundation, 20th Annual Research Conference, pp. 402-421.

Johannessen, E.P., Steel, R.J., 2005. Shelf-margin clinoforms and prediction of deepwater sands. Basin Research 17, 521-550.

Johnston, D., Player, W., Gregg, R., Cook, R., 1996. New Zealand: All the Right Ingredients. Petroleum Exploration Society of Australia (PESA) 22.

Kennett, J.P., Houtz, R.E., Andrews, P.B., Edwards, A.R., Edwards, A.R., Gostin, V.A., Hajos, M., Hampton, D.G., Jenkins, S.G., Margolis, S.V., Ovenshine, A.T., Perchnielsen, K., 1975. Cenozoic Paleoceanography in the Southwest Pacific Ocean, Antarctic Galciation, and the Development of the Circum-Antarctic Current. Technical Report. In: Initial Reports of the Deep Sea Drilling Project, vol. 2.

Kennett, J.P., Stott, L.D., 1990. Proteus and Proto-Oceanus: ancestral Paleogene oceans as revealed from Antarctic stable isotope results: ODP Leg 113. Proc. ODP Sci. Results 113, 865–880

Killops, S.D., Cook, R.A., Sykes, R., Boudou, J.P., 1997. Petroleum potential and oil-source correlation in the Great South and Canterbury Basins. New Zealand Journal of Geology and Geophysics 40, 405-423.

Killops, S.D., Hollis, C.J., Morgans, H.E.G., Sutherland, R., Field, B.D., Leckie, D.A., 2000. Paleoceanographic significance of Late Paleocene dysaerobia at the shelf/slope break around New Zealand. Palaeogeography, Palaeoclimatology, Palaeoecology 156, 51-70.

Knutz, P.C., 2008. Chapter 24: Palaeoceanographic Significance of Contourite Drifts, in: Rebesco, M., Camerlenghi, A. (Eds.), Developments in Sedimentology. Elsevier, pp. 511-535.

Knutz, P., Cartwright, J., 2004. 3D anatomy of late Neogene contourite drifts and associated mass flows in the Faroe-Shetland Basin. In: 3D Seismic Technology: Application to the Exploration of Sedimentary Basins, pp. 63-71.

Laberg, J.S., Stoker, M.S., Dahlgren, K.I.T., Haas, H.d., Haflidason, H., Hjelstuen, B.O., Nielsen, T., Shannon, P.M., Vorren, T.O., van Weering, T.C.E., Ceramicola, S., 2005. Cenozoic alongslope processes and sedimentation on the NW European Atlantic margin. Marine and Petroleum Geology 22, 1069-1088.

Lamb, S., 2011. Cenozoic tectonic evolution of the New Zealand plate-boundary zone: A paleomagnetic perspective. Tectonophysics 509, 135-164.

Lever, H., 2007. Review of unconformities in the late Eocene to early Miocene successions of the South Island, New Zealand: Ages, correlations, and causes. New Zealand Journal of Geology and Geophysics 50, 245-261.

Li, X., Fairweather, L., Wu, S., Ren, J., Zhang, H., Quan, X., Jiang, T., Zhang, C., Su, M., He, Y., Wang, D., 2013. Morphology, sedimentary features and evolution of a large palaeo submarine canyon in Qiongdongnan basin, Northern South China Sea. Journal of Asian Earth Sciences 62, 685-696.

Liu, Q., Zhu, X., Yang, Y., Geng, M., Tan, M., Jiang, L., Chen, L., 2016. Sequence stratigraphy and seismic geomorphology application of facies architecture and sediment-dispersal patterns analysis in the third

member of Eocene Shahejie Formation, slope system of Zhanhua Sag, Bohai Bay Basin, China. Marine and Petroleum Geology 78, 766-784.

Lonergan, L., Jamin, N.H., Jackson, C.A.L., Johnson, H.D., 2013. U-shaped slope gully systems and sediment waves on the passive margin of Gabon (West Africa). Marine Geology 337, 80-97.

Luyendyk, B.P., 1995. Hypothesis for Cretaceous rifting of east Gondwana caused by subducted slab capture. Geology 23, 373-376.

Lyle, M., Gibbs, S., Moore, T.C., Rea, D.K., 2007. Late Oligocene initiation of the Antarctic Circumpolar Current: evidence from the South Pacific. Geology 35, 691–694. doi:10.1130/23806A.1.

Masson, D., Harbitz, C., Wynn, R., Pedersen, G., Løvholt, F., 2006. Submarine landslides: processes, triggers and hazard prediction. Philosophical Transactions of the Royal Society of London A: Mathematical, Physical and Engineering Sciences 364, 2009-2039.

Mayall, M., Jones, E., Casey, M., 2006. Turbidite channel reservoirs—Key elements in facies prediction and effective development. Marine and Petroleum Geology 23, 821-841.

Mayall, M., Lonergan, L., Bowman, A., James, S., Mills, K., Primmer, T., Pope, D., Rogers, L., Skeene, R., 2010. The response of turbidite slope channels to growth-induced seabed topography. Bull. Am. Assoc. Hist. Nurs. 94, 1011–1030.

Mitchum Jr, R., Vail, P., Sangree, J., 1977. Seismic stratigraphy and global changes of sea level: Part 6. Stratigraphic interpretation of seismic reflection patterns in depositional sequences: Section 2. Application of seismic reflection configuration to stratigraphic interpretation. AAPG Memoir 26.

Morley, C.K., Maczak, A., Rungprom, T., Ghosh, J., Cartwright, J.A., Bertoni, C., Panpichityota, N., 2017. New style of honeycomb structures revealed on 3D seismic data indicate widespread diagenesis offshore Great South Basin, New Zealand. Marine and Petroleum Geology 86, 140-154.

Mulder T， Alexander J., 2001. The physical character of subaqueous sedimentary density flows and their deposits. Sedimentology, 48, 269-299.

Mulder, T., Syvitski, J.P.M., Migeon, S., Faugères, J.-C., Savoye, B., 2003. Marine hyperpycnal flows: initiation, behavior and related deposits. A review. Marine and Petroleum Geology 20, 861-882.

Mulder, T., Chapron, E., 2011. Flood Deposits in Continental and Marine Environments: Character and Significance. in R. M. Slatt and C. Zavala, eds., Sediment transfer from shelf to deep water—Revisiting the delivery system: AAPG Studies in Geology 61, p. 1-30.

Mutti, E., Carminatti, M., 2012. Deep-water sands in the Brazilian offshore basins: AAPG Search and Discovery. article 30219 http://www.searchanddiscovery.com/documents/ 2012/30219mutti/ndx_mutti.pdf.

Myers, K., 2009. Organic-Rich Facies and Hydrocarbon Source Rocks, in: Emery, D., Myers, K. (Eds.), Sequence Stratigraphy. Blackwell Science Ltd.

Nicolo, M.J., Dickens, G.R., Hollis, C.J., Zachos, J.C., 2007. Multiple early Eocene hyperthermals: Their sedimentary expression on the New Zealand continental margin and in the deep sea. Geology 35, 699-702.

Ogiesoba, O., Hammes, U., 2012. Seismic interpretation of mass-transport deposits within the upper Oligocene Frio Formation, south Texas Gulf Coast. AAPG Bull. 96, 845–868.

Omosanya, K.O., Alves, T.M., 2013. Ramps and flats of mass-transport deposits (MTDs) as markers of seafloor strain on the flanks of rising diapirs (Espírito Santo Basin, SE Brazil). Marine Geology 340, 82-97.

Omosanya, K.O., 2018. Episodic fluid flow as a trigger for Miocene-Pliocene slope instability on the Utgard High, Norwegian Sea. Basin Research. Accepted Author Manuscript.

Patruno, S., Hampson, G.J., Jackson, C.A.L., 2015. Quantitative characterisation of deltaic and subaqueous clinoforms. Earth-Science Reviews 142, 79-119.

Posamentier, H., Vail, P., 1988. Eustatic controls on clastic deposition II—sequence and systems tract models. SEPM Special Publication 42.

Posamentier, H.W., 2005. Application of 3D seismic visualization techniques for seismic stratigraphy, seismic geomorphology and depositional systems analysis: examples from fluvial to deep-marine depositional environments. Geological Society, London, Petroleum Geology Conference series 6, 1565-1576.

Posamentier, H.W., Davies, R.J., Cartwright, J.A., Wood, L., 2007. Seismic geomorphology - an overview. Geological Society, London, Special Publications 277, 1-14.

Posamentier, H.W., Kolla, V., 2003. Seismic geomorphology and stratigraphy of depositional elements in deep-water settings. Journal of Sedimentary Research 73, 367-388.

Rankey, E.C., 2017. Seismic architecture and seismic geomorphology of heterozoan carbonates: Eocene-Oligocene, Browse Basin, Northwest Shelf, Australia. Marine and Petroleum Geology 82, 424-443.

Reading, H.G., Richards, M., 1994. Turbidite systems in deep-water basin margins classified by grain size and feeder system. AAPG Bull. 78, 792–822.

Rebesco, M., Camerlenghi, A., 2008. Contourite, in: Rebesco, M., Camerlenghi, A. (Eds.), Developments in Sedimentology. Elsevier, pp. xvii-xviii.

Rebesco, M., Hernández-Molina, F.J., Van Rooij, D., Wåhlin, A., 2014. Contourites and associated sediments controlled by deep-water circulation processes: State-of-the-art and future considerations. Marine Geology 352, 111-154.

Rebesco, M., Stow, D., 2001. Seismic expression of contourites and related deposits: a preface. Marine Geophysical Researches 22, 303-308.

Richardson, S.E.J., Davies, R.J., Allen, M.B., Grant, S.F., 2011. Structure and evolution of mass transport deposits in the South Caspian Basin, Azerbaijan. Basin Research 23, 702-719.

Sangree, J.B., Widmier, J.M., 1977. Seismic Stratigraphy and Global Changes of Sea Level, Part 9: Seismic Interpretation of Clastic Depositional Facies, in: Payton, C.E. (Ed.), Seismic Stratigraphy — Applications to Hydrocarbon Exploration. American Association of Petroleum Geologists.

Scarselli, N., McClay, K., Elders, C., 2016. Seismic geomorphology of cretaceous megaslides offshore Namibia (Orange Basin): Insights into segmentation and degradation of gravity-driven linked systems. Marine and Petroleum Geology 75, 151-180.

Shanley, K.W., McCabe, P.J., 1994. Perspectives on the sequence stratigraphy of continental strata. AAPG bulletin 78, 544-568.

Shanmugam, G., 2006. Deep-water Processes and Facies Models: Implications for Sandstone Petroleum Reservoirs. Handbook of Petroleum Exploration and Production, 5. Elsevier Science (496 pp.).

Sheriff, R.E., Geldart, L.P., 1995. Exploration seismology. Cambridge university press.

Solheim, A., Berg, K., Forsberg, C.F., Bryn, P., 2005. The Storegga Slide complex: Repetitive large scale sliding with similar cause and development. Marine and Petroleum Geology 22, 97–107.

Steel, R., Olsen, T., 2002. Clinoforms, clinoform trajectories and deepwater sands, Sequence-stratigraphic models for exploration and production: Evolving methodology, emerging models and application histories: Gulf Coast Section SEPM 22nd Research Conference, Houston, Texas, pp. 367-381.

Stow, D., Hernández-Molina, F., Llave, E., Bruno, M., García, M., del Rio, V.D., Somoza, L., Brackenridge, R., 2013. The Cadiz Contourite Channel: Sandy contourites, bedforms and dynamic current interaction. Marine Geology 343, 99-114.

Stow, D.A.V., Faugères, J.-C., Howe, J.A., Pudsey, C.J., Viana, A.R., 2002. Bottom currents, contourites and deep-sea sediment drifts: current state-of-the-art. Geological Society, London, Memoirs 22, 7-20.

Sutherland, R., Spasojevic, S., Gurnis, M., 2010. Mantle upwelling after Gondwana subduction death explains anomalous topography and subsidence histories of eastern New Zealand and West Antarctica. Geology 38, 155-158.

Uruski, C., Ilg, B., 2006. Preliminary Interpretation and Structural Modelling of DUN06 Seismic Reflection Data from Great South Basin, Offshore New Zealand. GNS Science Consultancy, 46.

Uruski, C., Kennedy, C., Harrison, T., Maslen, G., Cook, R., Sutherland, R., Zhu, H., 2007. Petroleum potential of the Great South Basin, New Zealand—New seismic data improves imaging. The APPEA Journal 47, 145-161.

Uruski, C.I., 2010. New Zealand's deepwater frontier. Marine and Petroleum Geology 27, 2005-2026.

Vakarelov, B.K., Ainsworth, R.B., MacEachern, J.A., 2012. Recognition of wave-dominated, tide-influenced shoreline systems in the rock record: Variations from a microtidal shoreline model. Sedimentary Geology 279, 23-41.

Viskovic, G.P.D., 2011. Investigation of Fluid Migration Pathways in the Shallow Subsurface of the Great South Basin, through the use of High-Resolution Seismic Imaging of Fault and Fracture Systems. University of Otago.

Walker, R.G., 1992. Facies, facies models and modern stratigraphic concepts, in: Walker, R.G., James, N.P. (Eds.), Facies models: Response to sea-level change. Geological Association of Canada, Canada, pp. 1-14.

Ward, N.I.P., Alves, T.M., Blenkinsop, T.G., 2018. Submarine sediment routing over a blocky mass-transport deposit in the Espírito Santo Basin, SE Brazil. Basin Research 0.

Weaver, S.D., Storey, B.C., Pankhurst, R.J., Mukasa, S.B., Di Venere, V.J., Bradshaw, J.D., 1994. Antarctica-New Zealand rifting and Marie Byrd Land lithospheric magmatism linked to ridge subduction and mantle plume activity. Geology 22, 811-814.

Yilmaz, O., 2001. Seismic data analysis: Processing, inversion, and interpretation of seismic data: SEG.

Zavala, C., Arcuri, M., Di Meglio, M., Diaz, H.G., Contreras, C., 2011. A genetic facies tract for the analysis of sustained hyperpycnal flow deposits, in: Slatt, R.M., Zavala, C. (Eds.), Sediment transfer from shelf to deep water—Revisiting the delivery system: AAPG Studies in Geology 61. AAPG, Oklahoma, pp. 31-51.

Zeng, H., Backus, M.M., Barrow, K.T., Tyler, N., 1998. Stratal slicing, Part I: Realistic 3-D seismic model. GEOPHYSICS 63, 502-513.

Figure Captions

Fig. 1: Map showing the location of the Great South Basin (GSB) on the southern continental shelf of New Zealand. The purple polygon shows the location of the 3-D seismic dataset used for this study. In addition, the Pakaha-1 well was used for seismic-to-well tie and regional correlation across the 2-D seismic lines. (b) The outline of the 3-D seismic data and 2-D seismic profiles (Blue polygon) were used for this study. The spatial extent of the three mass-transport deposits (MTDs) discussed in the text is also shown. These MTDs have inferred headwall domains in the western part of the study area.

Fig. 2: Geodynamic evolution of the Southwestern Pacific region from the Triassic to Recent period. The eastern Gondwana margin was characterised by the southwest-dipping subduction of the Pacific–Phoenix plate from the Triassic to Early Cretaceous (>100 Ma). (a) and (b) The region experienced widespread intracontinental rifting (breakup) and extension from 100–85 Ma. (b) and (c) The period between 85-50 Ma corresponds to the opening of the Tasmanian Sea and isolation of Zealandia, which was followed by (d) and (e) the Cenozoic initiation and evolution of Tonga–Kermadec subduction from 50-0 Ma. The map is redrawn from Bache et al., 2014.

Fig. 3: W-E seismic profile showing the ages and formation of the interpreted horizons. The inset shows the location of the seismic profile. MTD- Mass-transport deposit, LAP-Lateral Accretion Package. (b) Age and lithology information were obtained from the Pakaha-1 well. (c) The time-depth (T-D) relationship is used for the depth conversion of structural maps. Note: Horizons designated as U1, U3 and U4 represent the tops and bases of Eocene deltaic systems.

Fig. 4: W-E seismic section showing the principal sediment types interpreted in the study area. These include three mass-transport deposits and three packages composed of deltaic clinoforms and contouritic deposits. The seismic profile shows that the underlying unit in the study area are severely faulted during Cretaceous rifting. The inset shows the location of the seismic profile. Note: Horizons designated as U1 to U6 represent the tops and bases of three Eocene deltaic systems. The red arrows show the direction of progradation of the deltaic clinoforms.

Fig. 5: W-E seismic section showing the chaotic nature of the MTD 1 and MTD 2. In addition, the complex nature of faults underlies the Cenozoic interval. The Marshal Paraconformity overlies the top of most of the polygonal fault system located in the southern part of the study area. The inset shows the location of the seismic profile. Note: Horizons U1 and U2 are the top and base of the oldest Eocene deltaic system interpreted in the study area.

Fig. 6: (a) & (b) Seismic section through MTD 1 and 2 showing their chaotic internal configurations and association with normal faults in the study area.

Fig. 7: Variance time slice at a depth of -1140 ms TWTT showing the outline of MTD 3 in association with the contourite mound, the canyon system and the polygonal fault systems. Blue arrows show the direction of mass transport for the MTD, while the black lines are composite lines for the seismic section

in Fig. 8. The black dashed lines mark the northern and southern limits of MTD 3 PFS-Polygonal Fault System.

Fig. 8: (a) & (b) Composite seismic sections and line drawings through MTD 3. The MTD show a strong affinity with the underlying polygonal fault systems and displayed distinctive characteristics such as a ridged-wavy top, an internal configuration that includes remnant blocks, slumps and chaotic seismic reflections. Importantly, the upper part of the MTD is characterized by a wide, large canyon system. See Fig. 7 for the location of the seismic sections.

Fig. 9: (a) & (b) Uninterpreted and interpreted seismic sections showing clinoforms and clinothems within Clinoform 1. The clinoforms are sigmoidal in shape. The upper boundary of the series is marked by horizon U2 while the base is delimited by horizon U1. The inset shows the location of the seismic profile. Note the changing vertical position between the clinoforms tops. (c) Flattening along the inferred maximum flooding surface shows that the clinoforms have a general 'ascending-descending-ascending' trajectory. Note: The interpreted clinothems are labelled alphabetically (d) The red rectangle shows the main shoreline trajectory classes of Helland-Hansen and Hampson (2009). Note: The red arrows show the direction of progradation of the deltaic clinoforms.

Fig. 10: (a) & (b) Uninterpreted and interpreted seismic sections showing complex sigmoid to oblique clinoforms and clinothems within Clinoform 2. Horizons U3 and U4 are at the upper and lower boundaries of the sequence, respectively. The inset shows the location of the seismic profile. Note the changing vertical position between the clinoforms tops. (c) The flattening of U3 shows that clinoforms have a descending - ascending trajectory. Note: the interpreted clinothems are labelled alphabetically. (d) The red rectangle shows the main shoreline trajectory classes of Helland-Hansen and Hampson (2009). Note: The red arrows show the direction of progradation of the deltaic clinoforms.

Fig. 11: (a) & (b) Uninterpreted and interpreted seismic sections showing parallel-sigmoid clinoforms and clinothems within Clinoform 3. The inset shows the location of the seismic profile. Note the changing vertical position between the clinoforms tops. (c) The clinoforms have an ascending to descending trajectory. Note: The interpreted clinothems are labelled alphabetically. (d) The red rectangle shows the main shoreline trajectory classes of Helland-Hansen and Hampson (2009). Note: The red arrows show the direction of progradation of the deltaic clinoforms.

Fig. 12: Isopach map of (a) Clinoform 1 (depositional sequence U1 to U2). The map shows that the sequence generally thickens to the NE part of the study area. (b) Clinoform 2 (depositional sequence U3 to U4). The sedimentary package or clinothems within Clinoform 2 cumulatively thicken to the SE part of the study area. (c) A similar trend is noted for Clinoform 3 (depositional sequence U5 to U6), which thickens to the SE part of the study area. (d) U1 to U6. This map indicates a general NE direction of transport for Clinoforms 1 to 3. In addition to the isopach, the interpreted positions of the clinoform's geomorphologic divisions such as topset, foreset and bottomset are also indicated. Note: Contour spacing for the maps is 50 m, while the arrows signify the inferred direction of sediment transport

Fig. 13: Variance time slices showing sediment conduits and depositional components associated with Clinoform 1 to Clinoform 3. (a) The channels interpreted here are generally oriented in an SE direction. The associated lobes or fans are interpreted as areas of low variance coefficients surrounding the channels. Lobes associated with Unit 1 are oriented in the NE, E and SE directions. (b) The channels interpreted here also show NW to SE orientations relative to an inferred lobe that is oriented to the north. Either the dashed red lines are interpreted as bottom currents perpendicular to the trend of the channels or the location of the paleo shorelines (c) The channels and lobe are oriented to the E and NE. Note: The inferred lobes are shown with dashed purple lines on the schematic diagrams while the question marks also indicate areas of high uncertainty. The southern part of the study area is complicated with no distinct features revealed on the maps; hence, it has been omitted here. (d) Tripartite classification of deltas into river-, wave-, and tide- dominated end members (Modified after: Bhattacharya, 2006; Galloway, 1975; Walker, 1992).

Fig: 14: Illustration showing the evolution of deltaic clinoforms in Clinoform 1 to Clinoform 3. The block diagrams show that the deltas were fed by fluvial channels, prograded over the shelf and are transported to the SE and NE parts from the Early Eocene to Mid Eocene. The dynamics and orientation of the channels and their lobes may be controlled by regional tectonics during the Eocene or nearshore currents.

Fig. 15: (a) & (b) Seismic section and corresponding line drawing through the main elongate contourite drifts interpreted in the study area. At the topmost part of the youngest drift is a chaotic and distorted package interpreted as a slump, which is in turn overlain by turbidite channels. (c) Structure maps of mounds and the locations of seismic sections shown in (a) and (b).

Fig. 16: (a) & (b) Seismic section and corresponding line drawing through the main elongate contourite drifts and their associated moats/channels. The contourite drifts extended outside the 3-D seismic data and were interpreted on the regional 2-D lines.

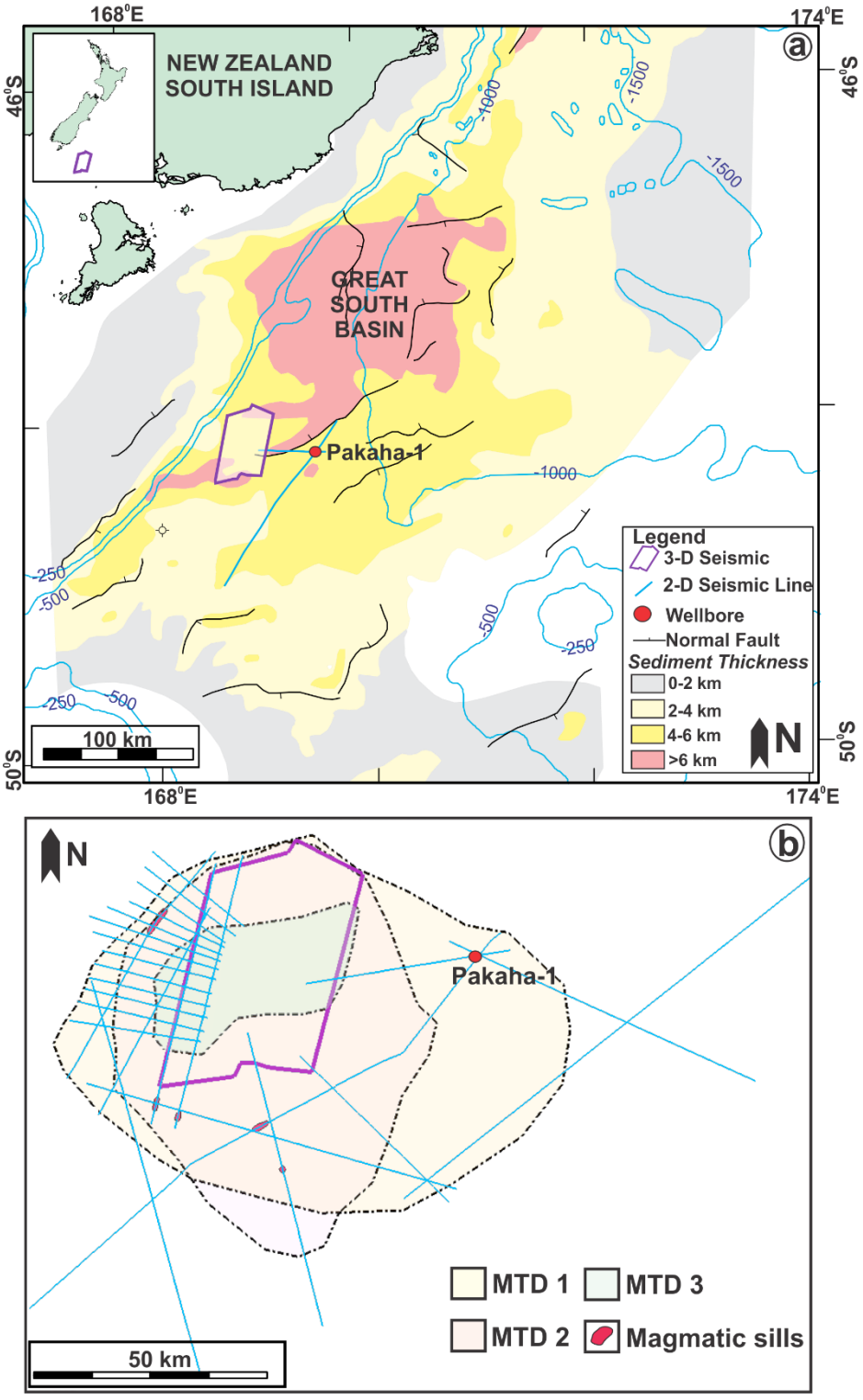
168°E
174°E
46°S
50°S
a
NEW ZEALAND
SOUTH ISLAND
GREAT
SOUTH
BASIN
Pakaha-1
-1000
-1500
-250
-500
Legend
3-D Seismic
2-D Seismic Line
Wellbore
Normal Fault
Sediment Thickness
0-2 km
2-4 km
4-6 km
>6 km
N
100 km
b
Pakaha-1
MTD 1
MTD 3
MTD 2
Magmatic sills
50 km

Fig1

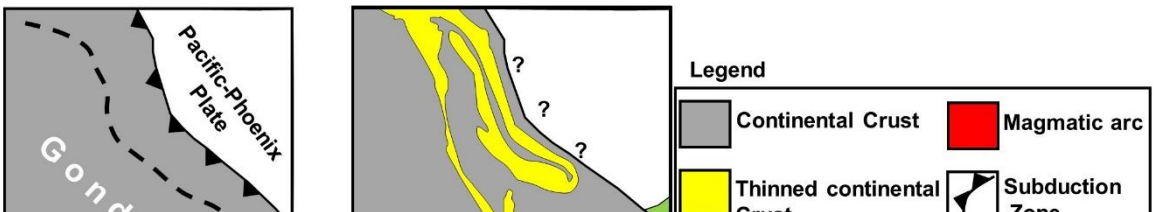
Pacific-Phoenix
Plate
?
Legend
Continental Crust
Magmatic arc
Thinned continental
Subduction

Fig. 2

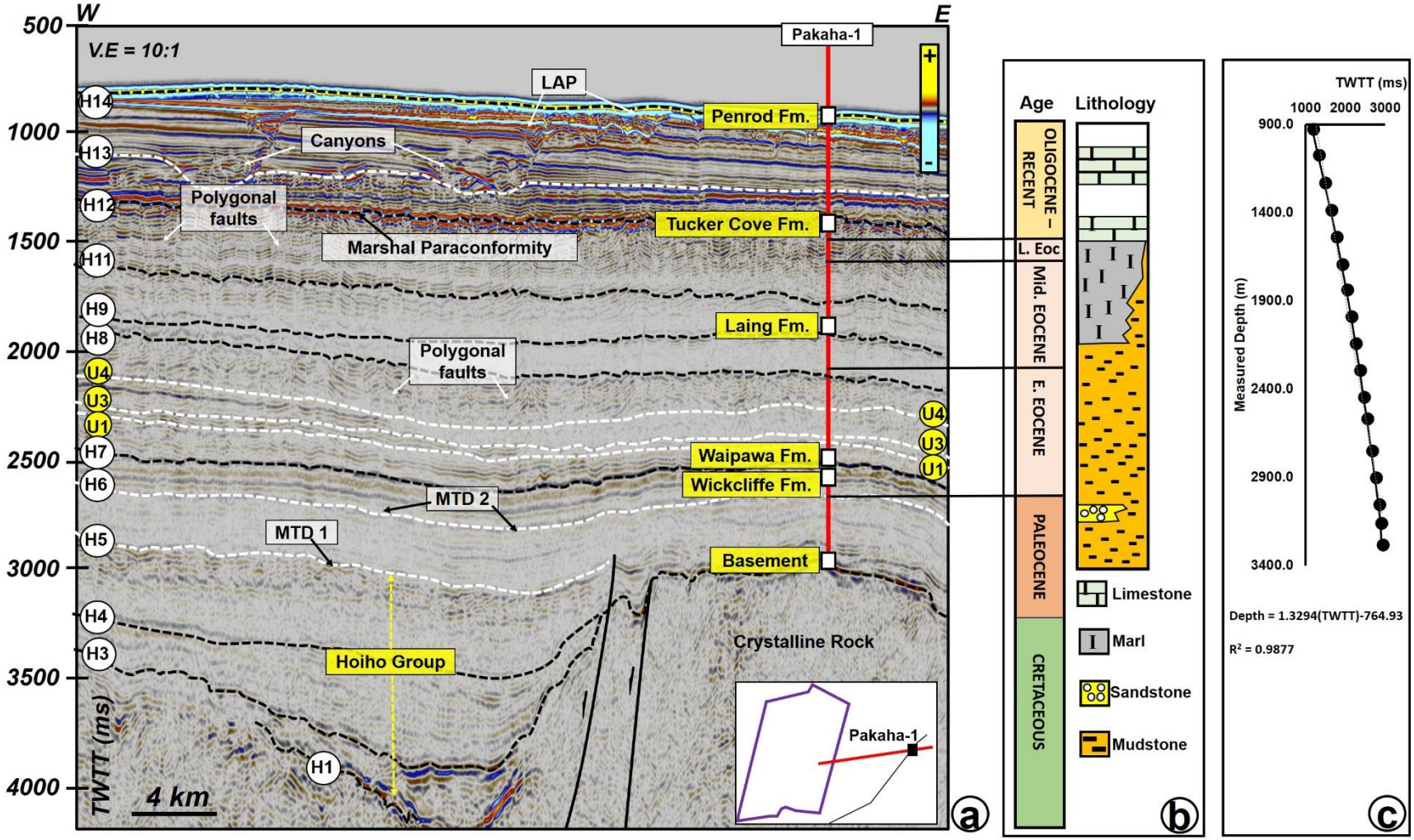
W
E
500
1000
1500
2000
2500
3000
3500
4000
V.E = 10:1
Pakaha-1
LAP
Penrod Fm.
Canyons
Polygonal faults
Marshal Paraconformity
Tucker Cove Fm.
Laing Fm.
Polygonal faults
Waipawa Fm.
Wickcliffe Fm.
MTD 2
MTD 1
Basement
Hoiho Group
Crystalline Rock
Pakaha-1
H14
H13
H12
H11
H9
H8
U4
U3
U1
H7
H6
H5
H4
H3
H1
TWTT (ms)
4 km
a
Age
Lithology
OLIGOCENE – RECENT
L. Eoc
Mid. EOCENE
E. EOCENE
PALEOCENE
CRETACEOUS
Limestone
Marl
Sandstone
Mudstone
b
TWTT (ms)
1000 2000 3000
900.0
1400.0
1900.0
2400.0
2900.0
3400.0
Measured Depth (m)
Depth = 1.3294(TWTT)-764.93
R² = 0.9877
c

Fig. 3

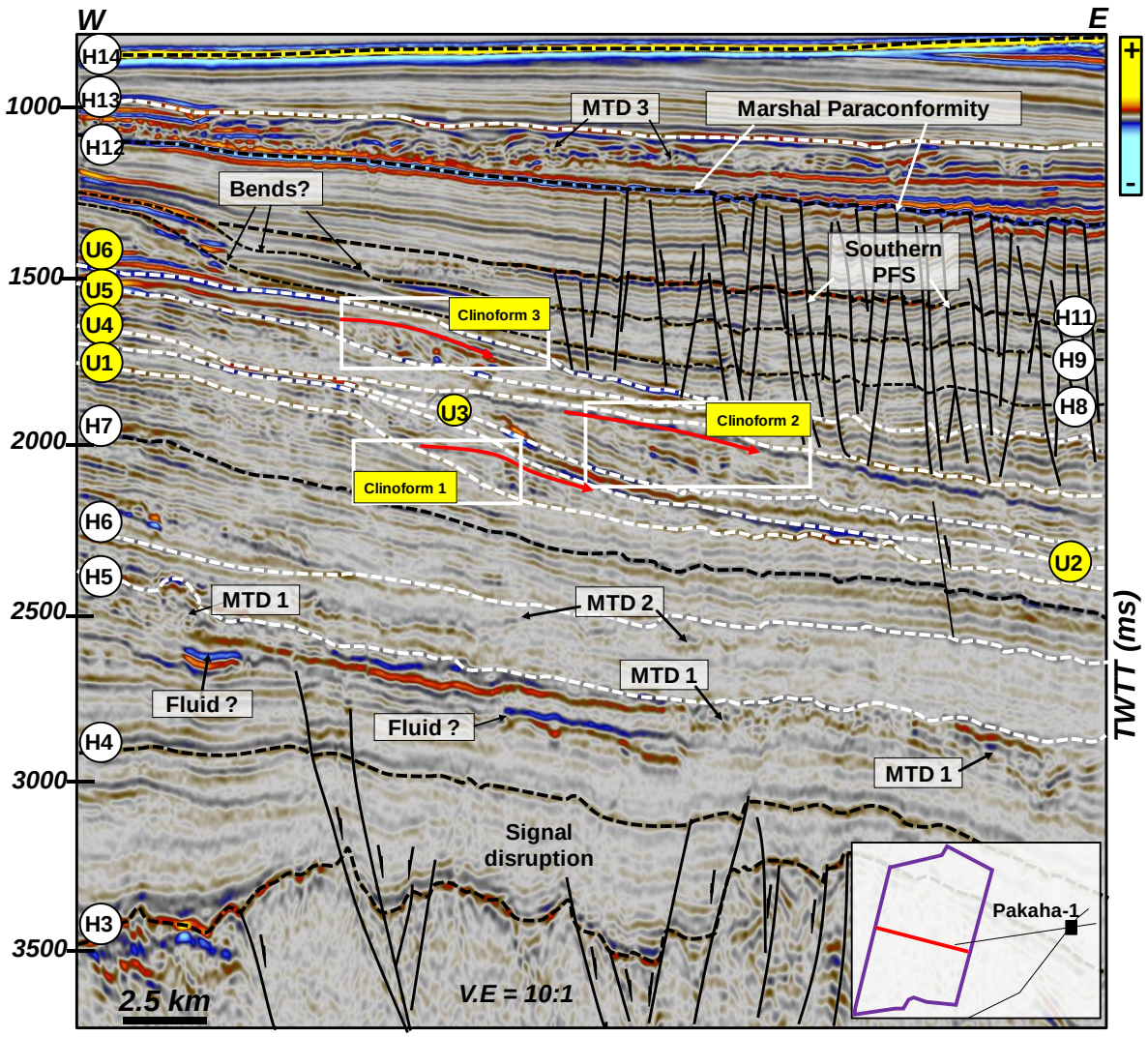
W
E
H14
H13
H12
1000
MTD 3
Marshal Paraconformity
Bends?
Southern
PFS
U6
1500
U5
U4
U1
Clinoform 3
H11
H9
H8
U3
Clinoform 2
H7
2000
Clinoform 1
H6
H5
U2
MTD 1
MTD 2
2500
MTD 1
Fluid ?
Fluid ?
H4
3000
MTD 1
Signal
disruption
H3
3500
Pakaha-1
2.5 km
V.E = 10:1
+
-
TWTT (ms)

Fig. 4

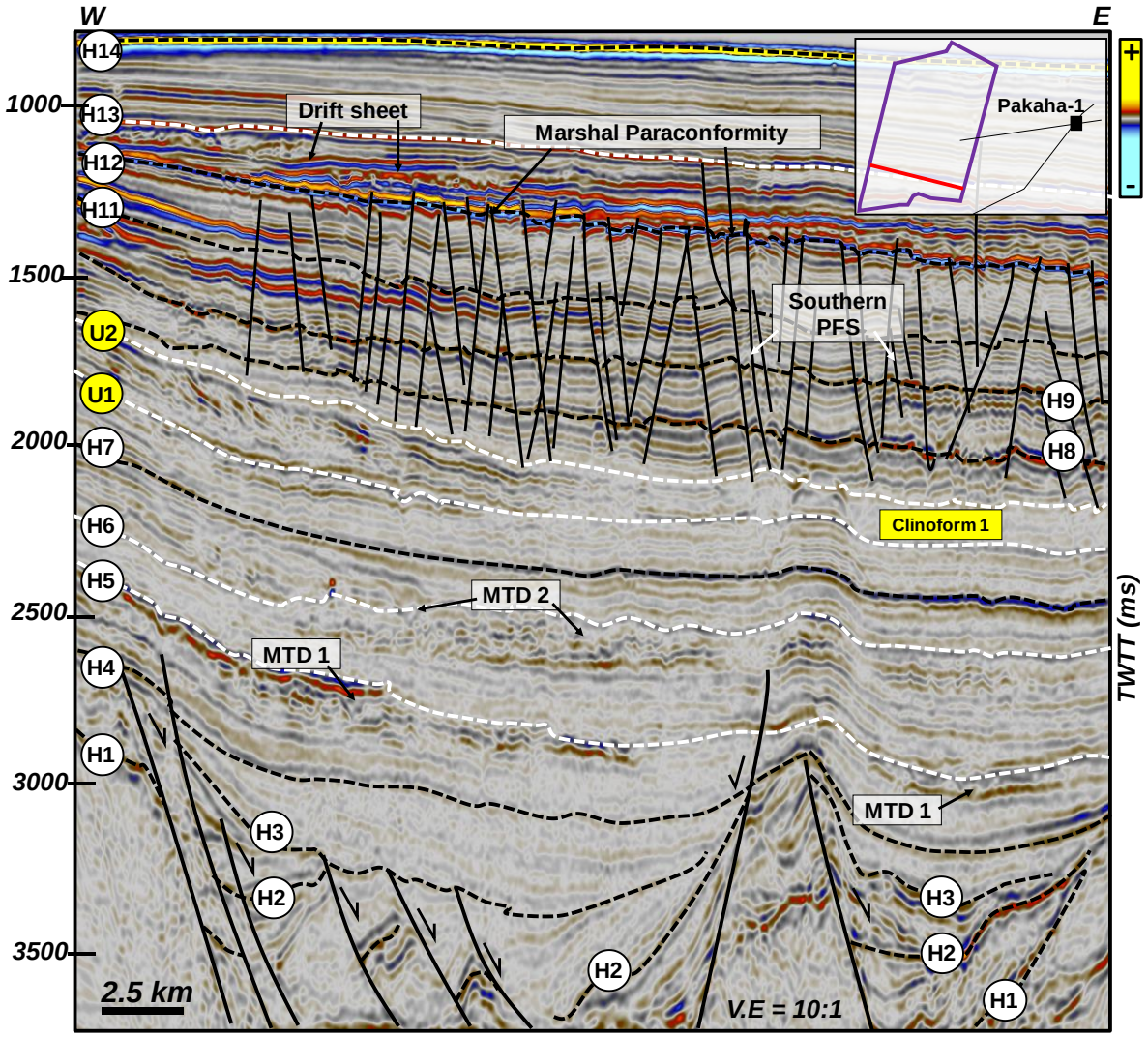
W
E
H14
H13
H12
H11
U2
U1
H7
H6
H5
H4
H1
1000
1500
2000
2500
3000
3500
Drift sheet
Marshal Paraconformity
Pakaha-1
+
-
Southern
PFS
H9
H8
Clinoform 1
MTD 2
MTD 1
MTD 1
H3
H2
H3
H2
H2
H1
2.5 km
V.E = 10:1
TWTT (ms)

Fig. 5

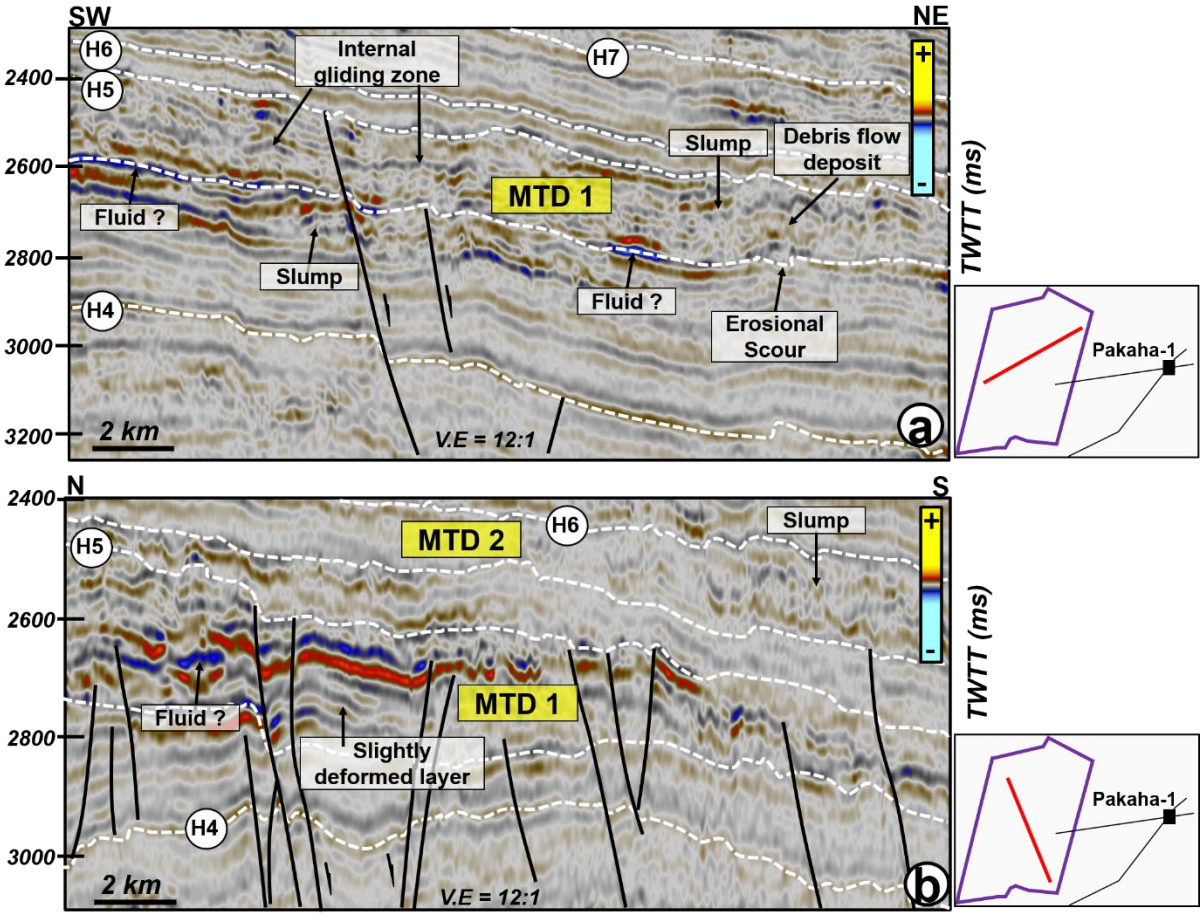
SW
NE
H6
H5
H7
Internal gliding zone
Slump
Debris flow deposit
MTD 1
Fluid ?
Slump
Fluid ?
Erosional Scour
H4
2400
2600
2800
3000
3200
2 km
V.E = 12:1
a
TWTT (ms)
Pakaha-1
N
S
MTD 2
H6
Slump
H5
MTD 1
Fluid ?
Slightly deformed layer
H4
2400
2600
2800
3000
2 km
V.E = 12:1
b
TWTT (ms)
Pakaha-1

Fig. 6

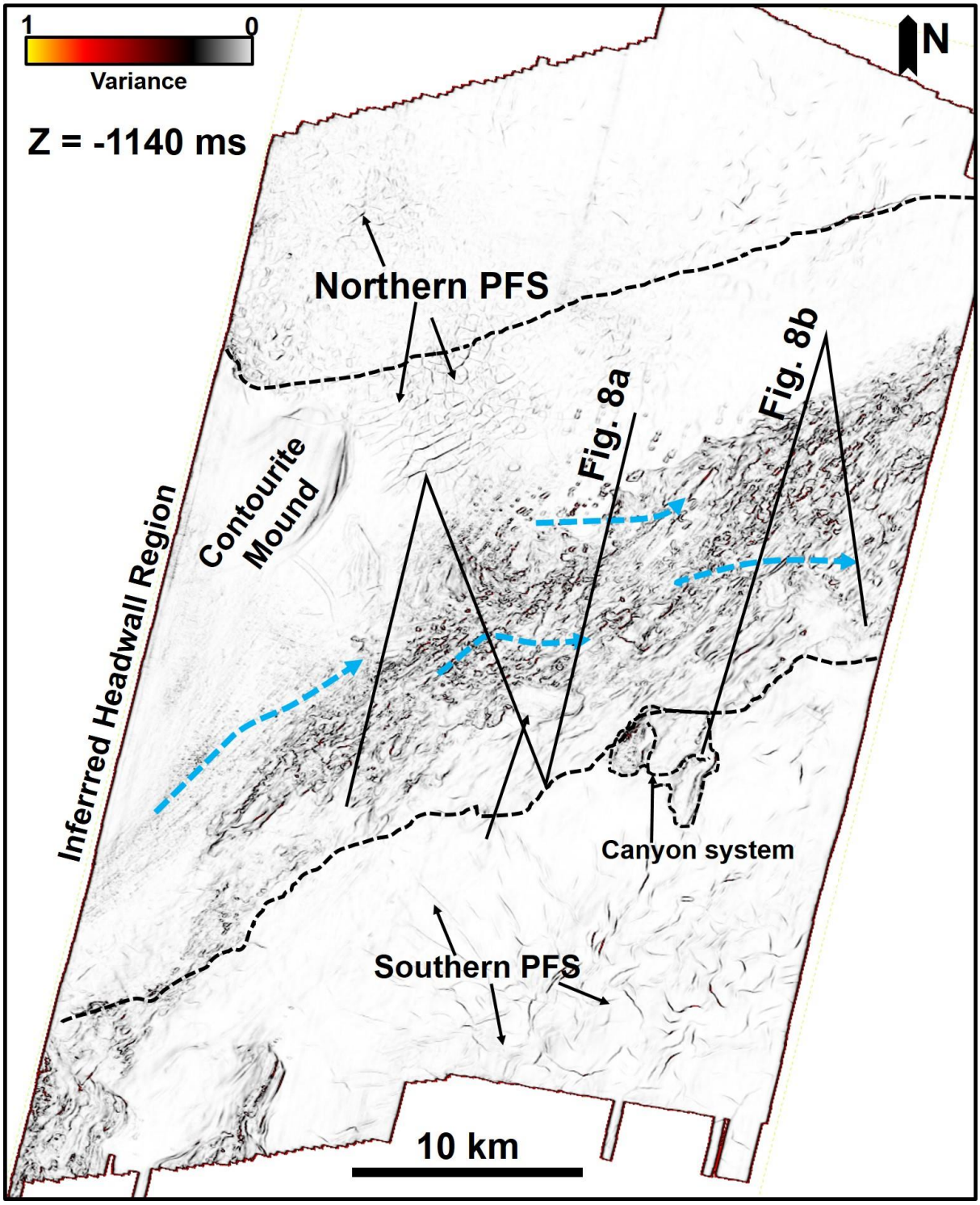
1
0
Variance
Z = -1140 ms
N
Northern PFS
Fig. 8a
Fig. 8b
Contourite Mound
Inferrred Headwall Region
Canyon system
Southern PFS
10 km

Fig. 7

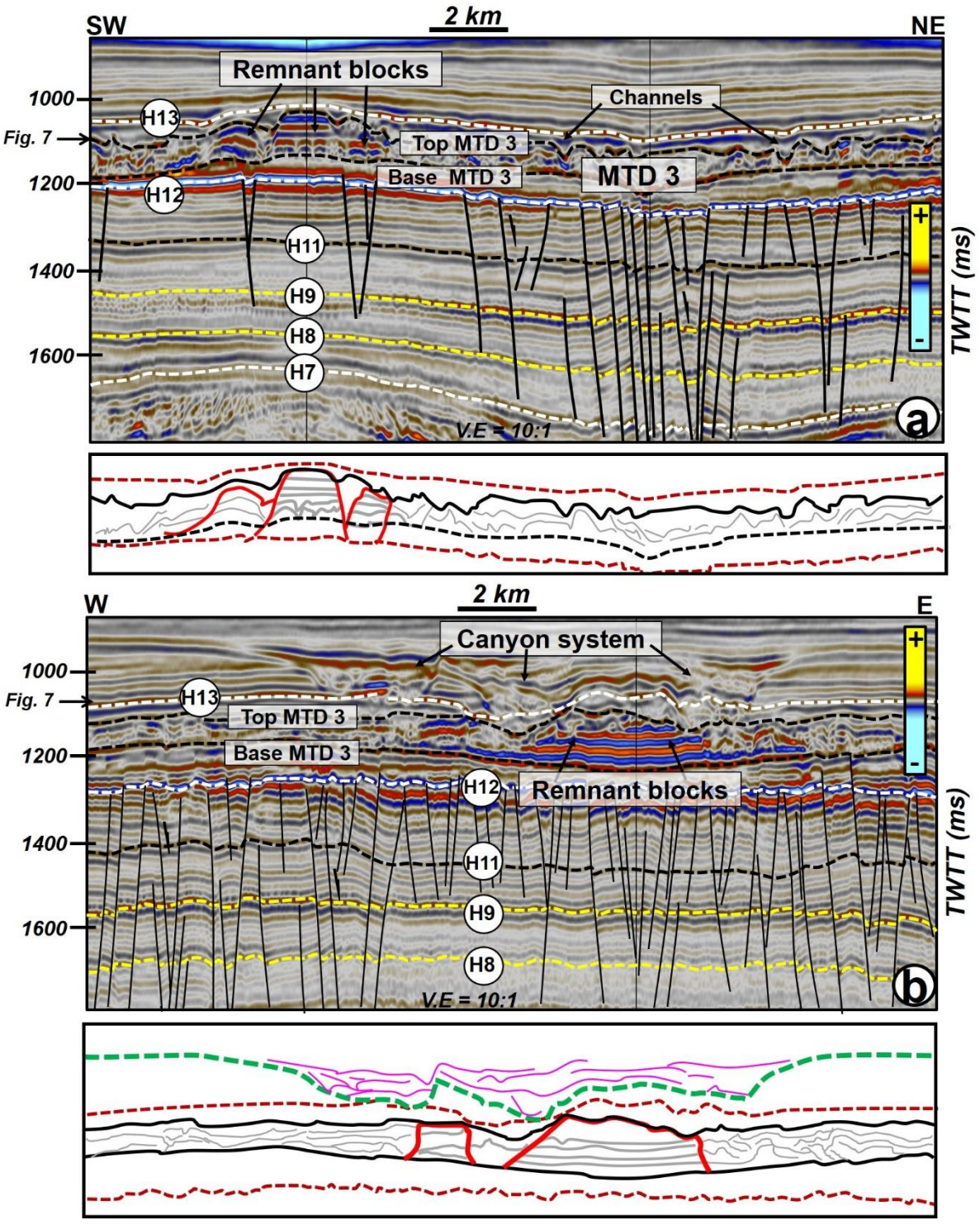
SW
2 km
NE
Remnant blocks
Channels
Top MTD 3
Base MTD 3
MTD 3
H13
H12
H11
H9
H8
H7
1000
1200
1400
1600
Fig. 7
V.E = 10:1
a
TWTT (ms)
W
2 km
E
Canyon system
Top MTD 3
Base MTD 3
Remnant blocks
H13
H12
H11
H9
H8
1000
1200
1400
1600
Fig. 7
V.E = 10:1
b
TWTT (ms)

Fig. 8

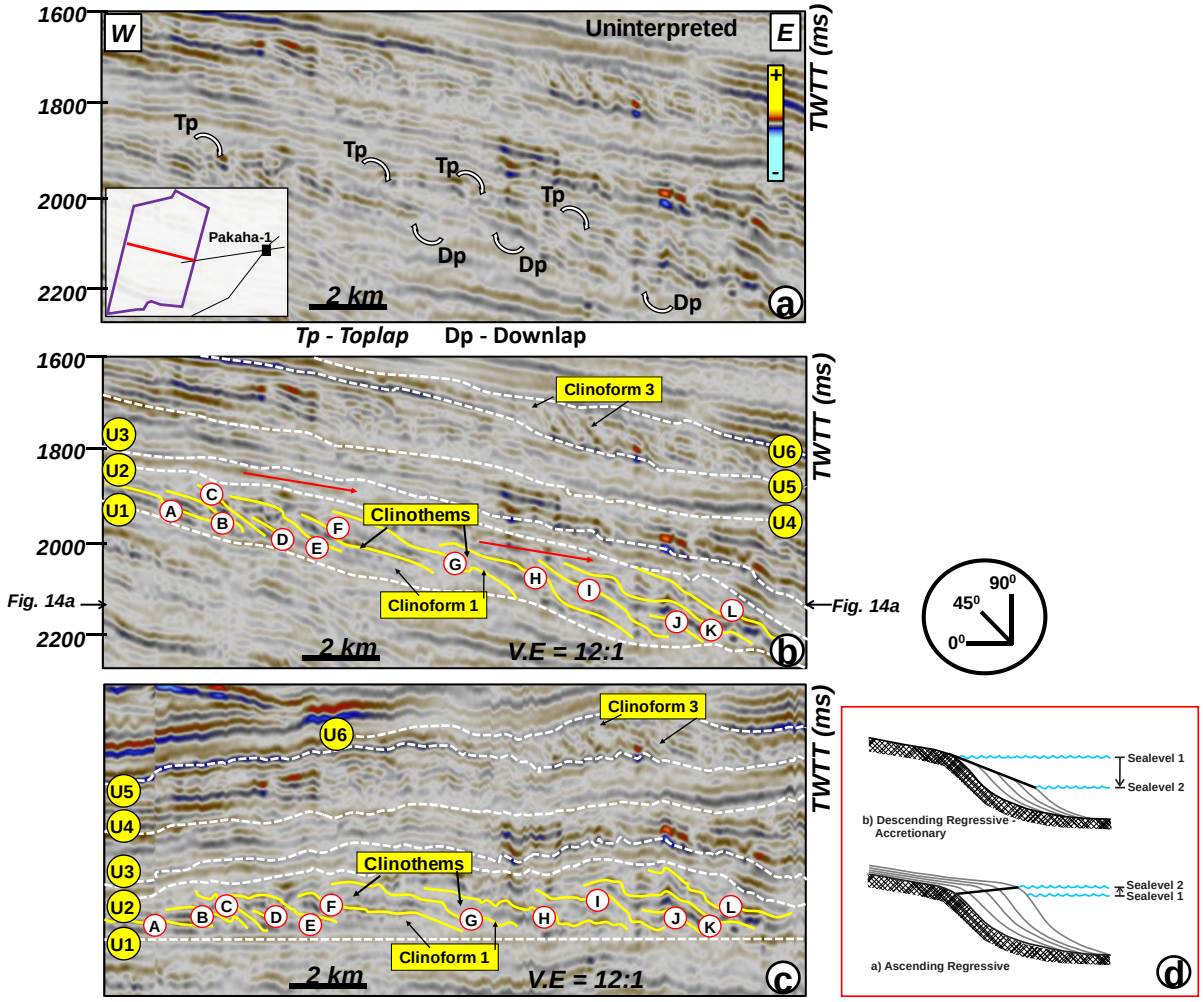
1600
1800
2000
2200
W
E
Uninterpreted
TWTT (ms)
Tp
Dp
Pakaha-1
2 km
a
Tp - Toplap
Dp - Downlap
Clinoform 3
U3
U2
U1
U6
U5
U4
A
B
C
D
E
F
G
H
I
J
K
L
Clinothems
Clinoform 1
Fig. 14a
V.E = 12:1
b
c
90⁰
45⁰
0⁰
Sealevel 1
Sealevel 2
b) Descending Regressive
Accretionary
a) Ascending Regressive
d

Fig. 9

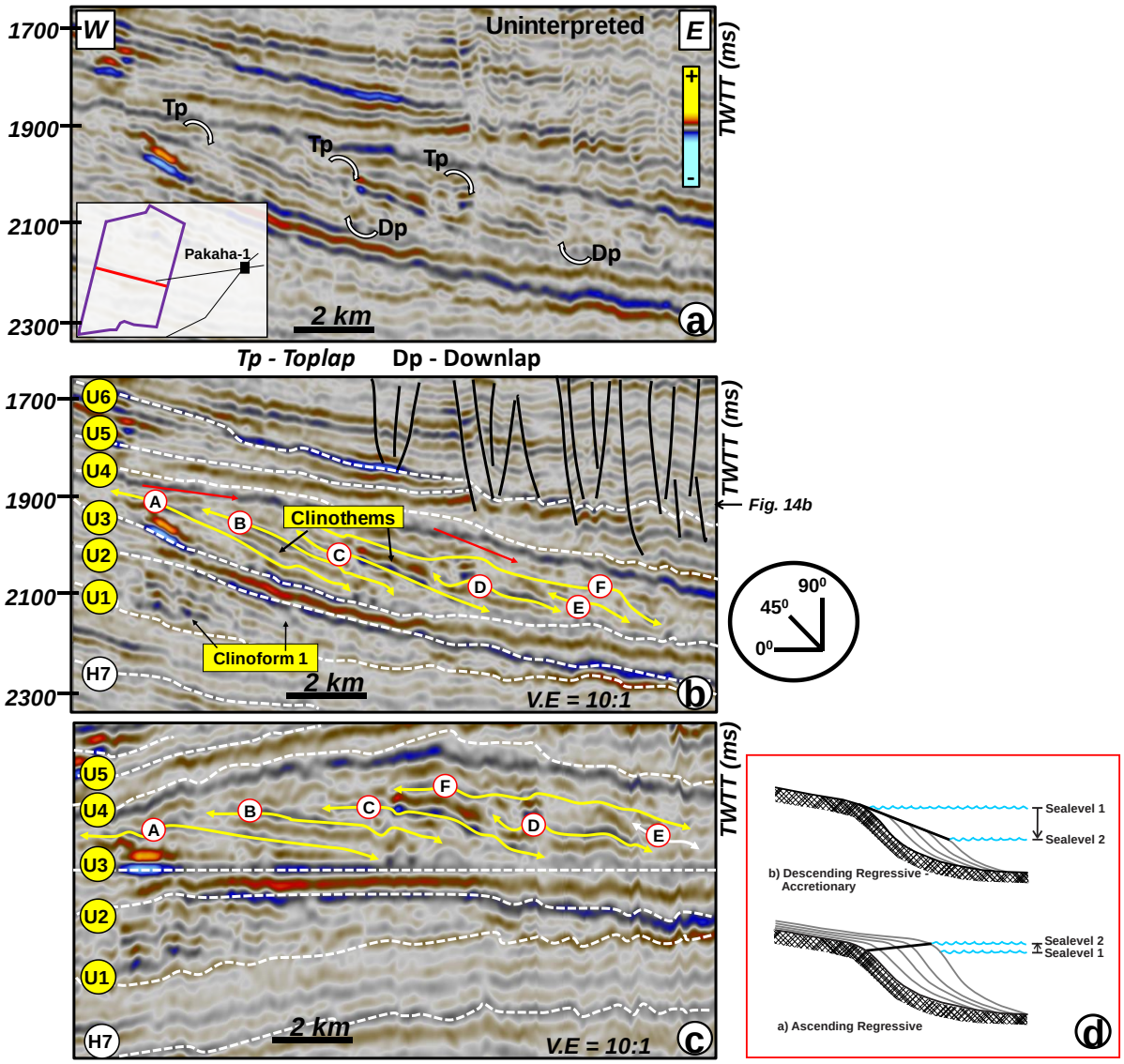
1700
1900
2100
2300
W
E
Uninterpreted
TWTT (ms)
Tp
Dp
Pakaha-1
2 km
a
Tp - Toplap
Dp - Downlap
U6
U5
U4
U3
U2
U1
H7
A
B
C
D
E
F
Clinothems
Clinoform 1
V.E = 10:1
b
Fig. 14b
90⁰
45⁰
0⁰
c
Sealevel 1
Sealevel 2
b) Descending Regressive - Accretionary
a) Ascending Regressive
d

Fig. 10

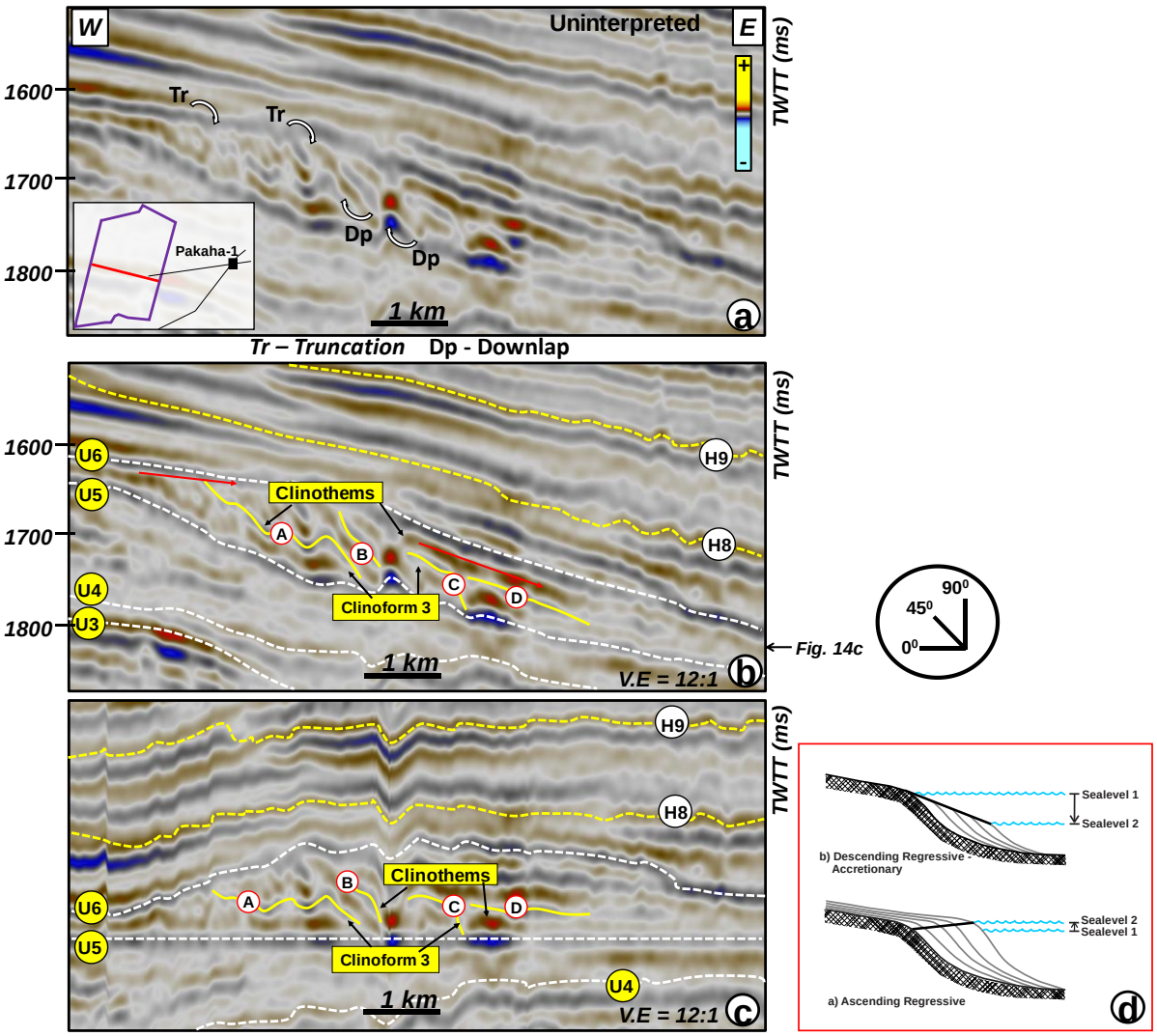
W
E
Uninterpreted
TWTT (ms)
1600
1700
1800
Tr
Tr
Dp
Dp
Pakaha-1
1 km
a
Tr – Truncation
Dp - Downlap
U6
U5
U4
U3
H9
H8
Clinothems
A
B
C
D
Clinoform 3
1 km
V.E = 12:1
b
Fig. 14c
90⁰
45⁰
0⁰
c
U4
b) Descending Regressive - Accretionary
Sealevel 1
Sealevel 2
a) Ascending Regressive
d

Fig. 11

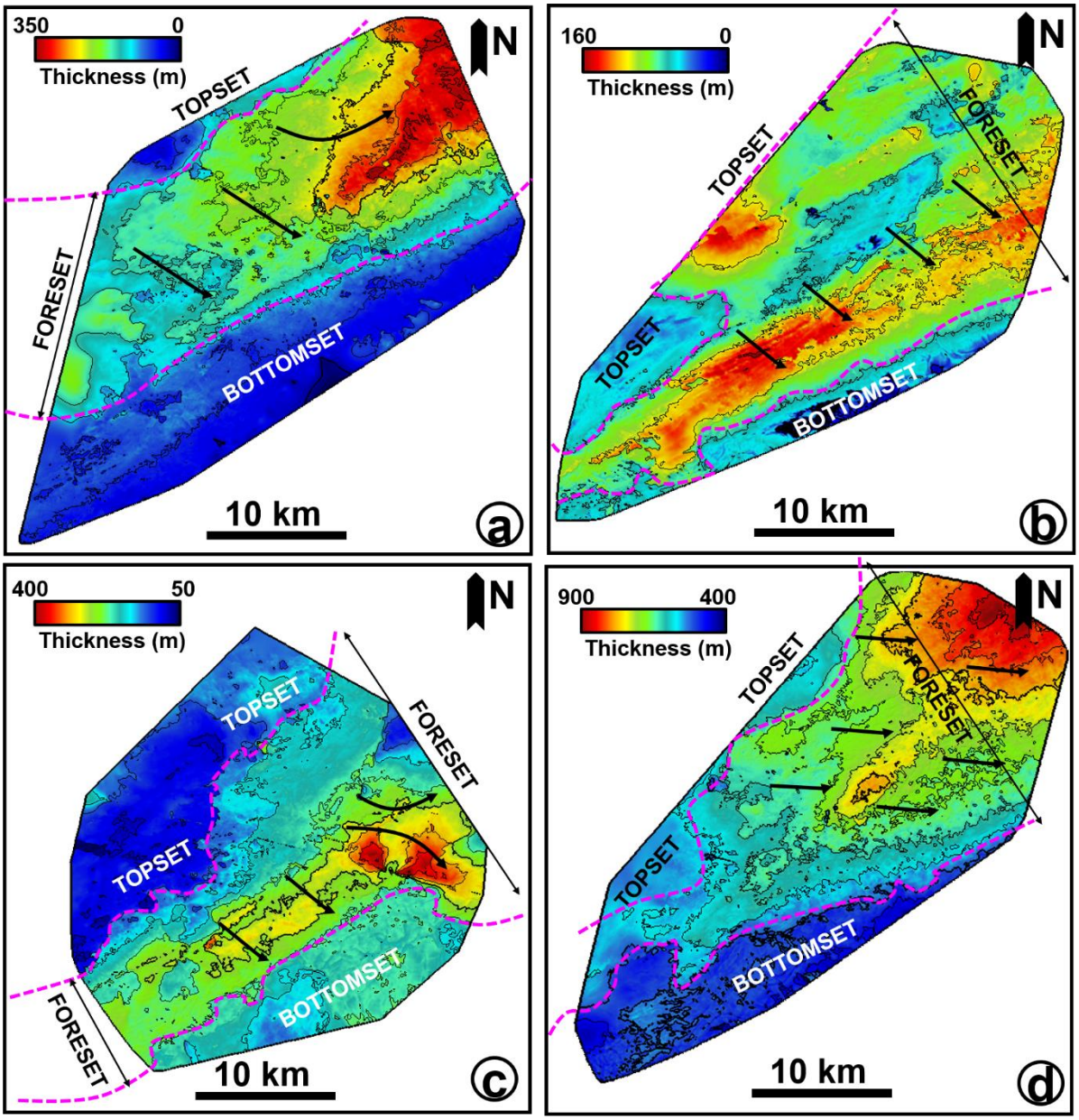
350
0
Thickness (m)
N
TOPSET
FORESET
BOTTOMSET
10 km
a
160
0
Thickness (m)
N
TOPSET
FORESET
BOTTOMSET
10 km
b
400
50
Thickness (m)
N
TOPSET
TOPSET
FORESET
FORESET
BOTTOMSET
10 km
c
900
400
Thickness (m)
N
TOPSET
TOPSET
FORESET
BOTTOMSET
10 km
d

Fig. 12

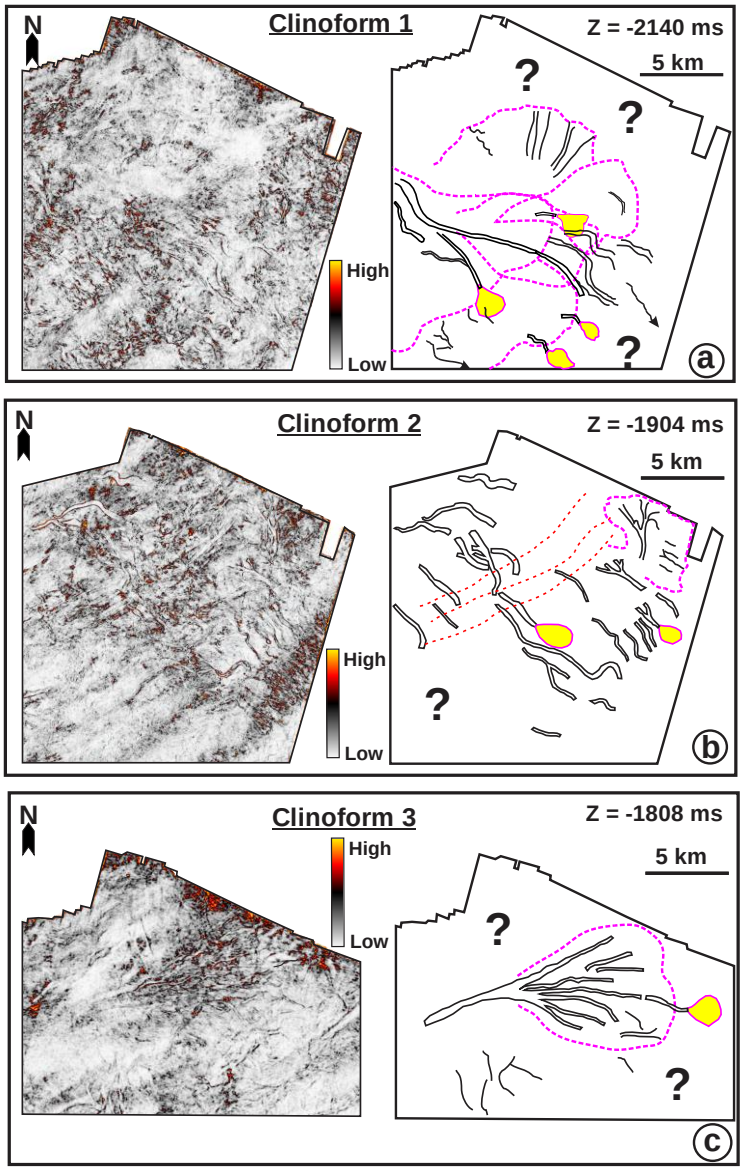
N
Clinoform 1
Z = -2140 ms
5 km
High
Low
?
?
?
a
N
Clinoform 2
Z = -1904 ms
5 km
High
Low
?
b
N
Clinoform 3
Z = -1808 ms
5 km
High
Low
?
c

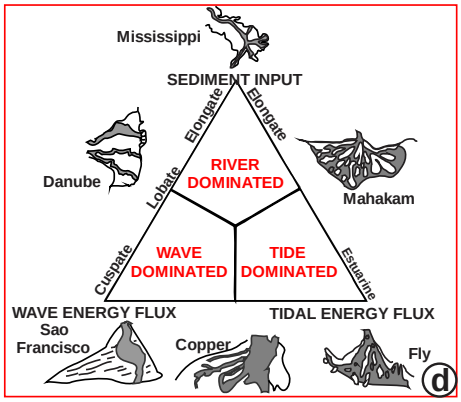
Mississippi
SEDIMENT INPUT
Elongate
Elongate
Lobate
Danube
RIVER
DOMINATED
Mahakam
Cuspate
WAVE
DOMINATED
TIDE
DOMINATED
Estuarine
WAVE ENERGY FLUX
TIDAL ENERGY FLUX
Sao
Francisco
Copper
Fly
d

Fig. 13

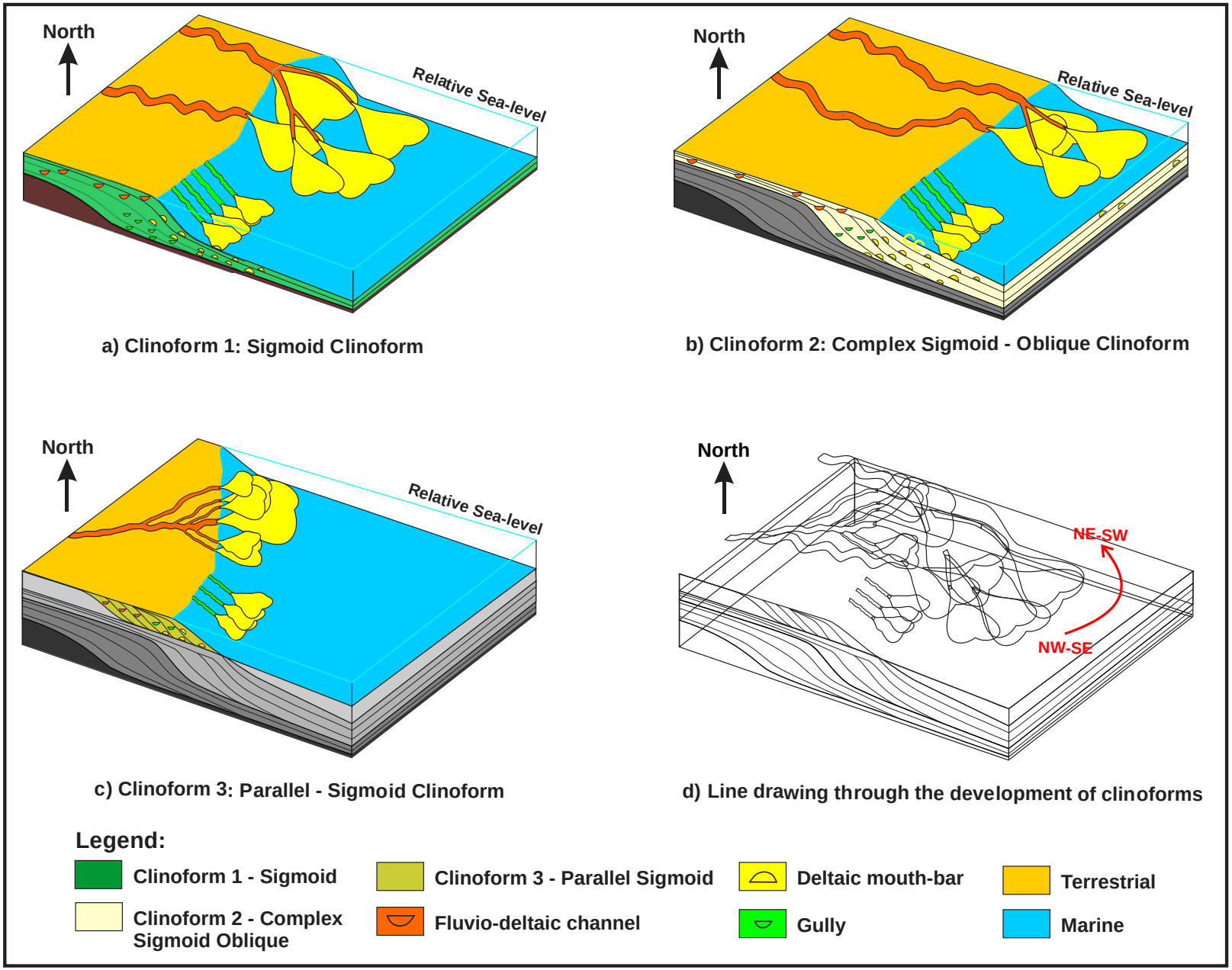
North
Relative Sea-level
a) Clinoform 1: Sigmoid Clinoform
North
Relative Sea-level
b) Clinoform 2: Complex Sigmoid - Oblique Clinoform
North
Relative Sea-level
c) Clinoform 3: Parallel - Sigmoid Clinoform
North
NE-SW
NW-SE
d) Line drawing through the development of clinoforms
Legend:
Clinoform 1 - Sigmoid
Clinoform 2 - Complex Sigmoid Oblique
Clinoform 3 - Parallel Sigmoid
Fluvio-deltaic channel
Deltaic mouth-bar
Gully
Terrestrial
Marine

Fig: 14

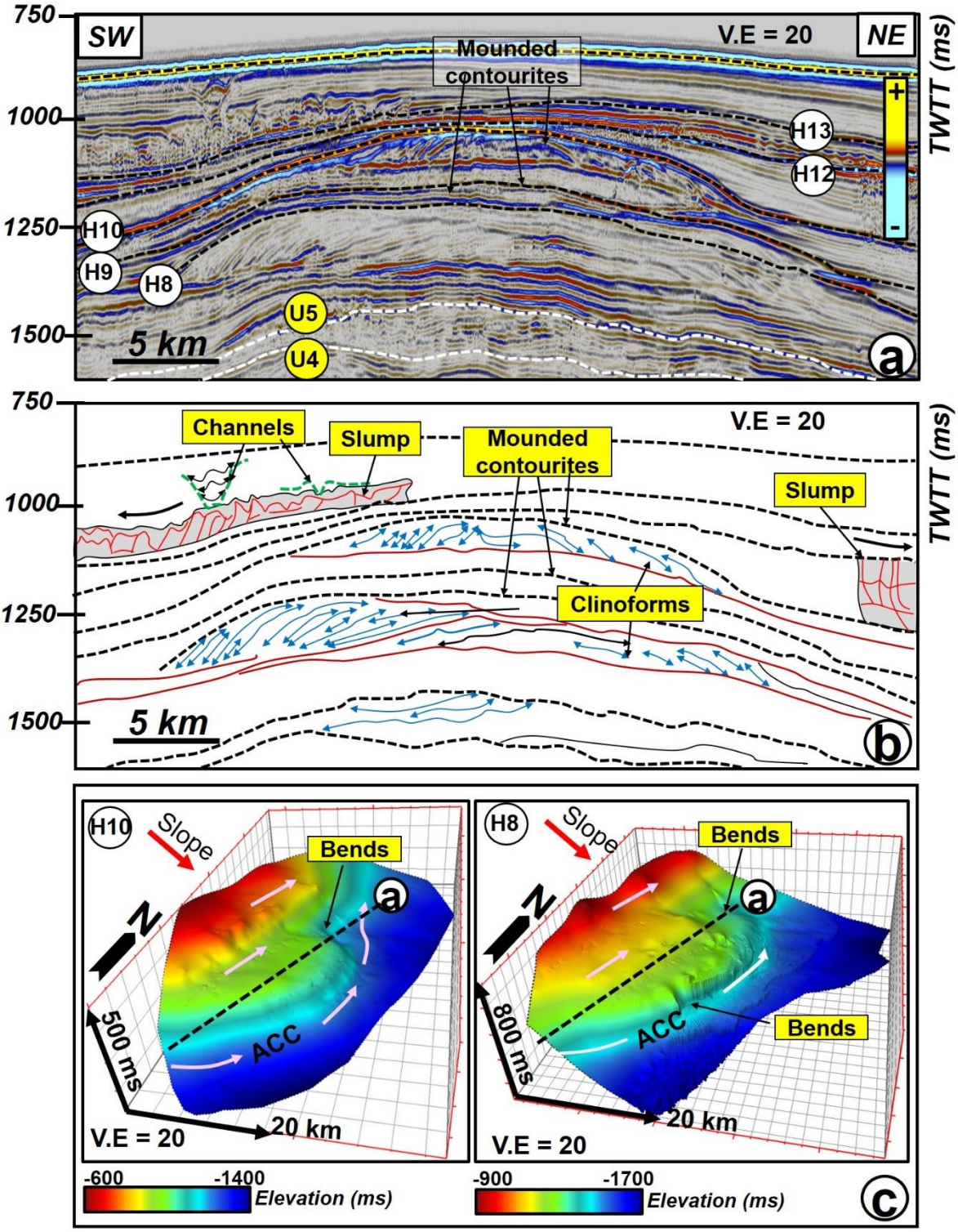
750
1000
1250
1500
SW
NE
V.E = 20
Mounded contourites
H13
H12
H10
H9
H8
U5
U4
5 km
a
TWTT (ms)
Channels
Slump
Mounded contourites
Slump
Clinoforms
5 km
b
H10
Slope
Bends
a
N
500 ms
ACC
20 km
V.E = 20
-600
-1400
Elevation (ms)
H8
Slope
Bends
a
N
800 ms
ACC
Bends
20 km
V.E = 20
-900
-1700
Elevation (ms)
c

Fig. 15

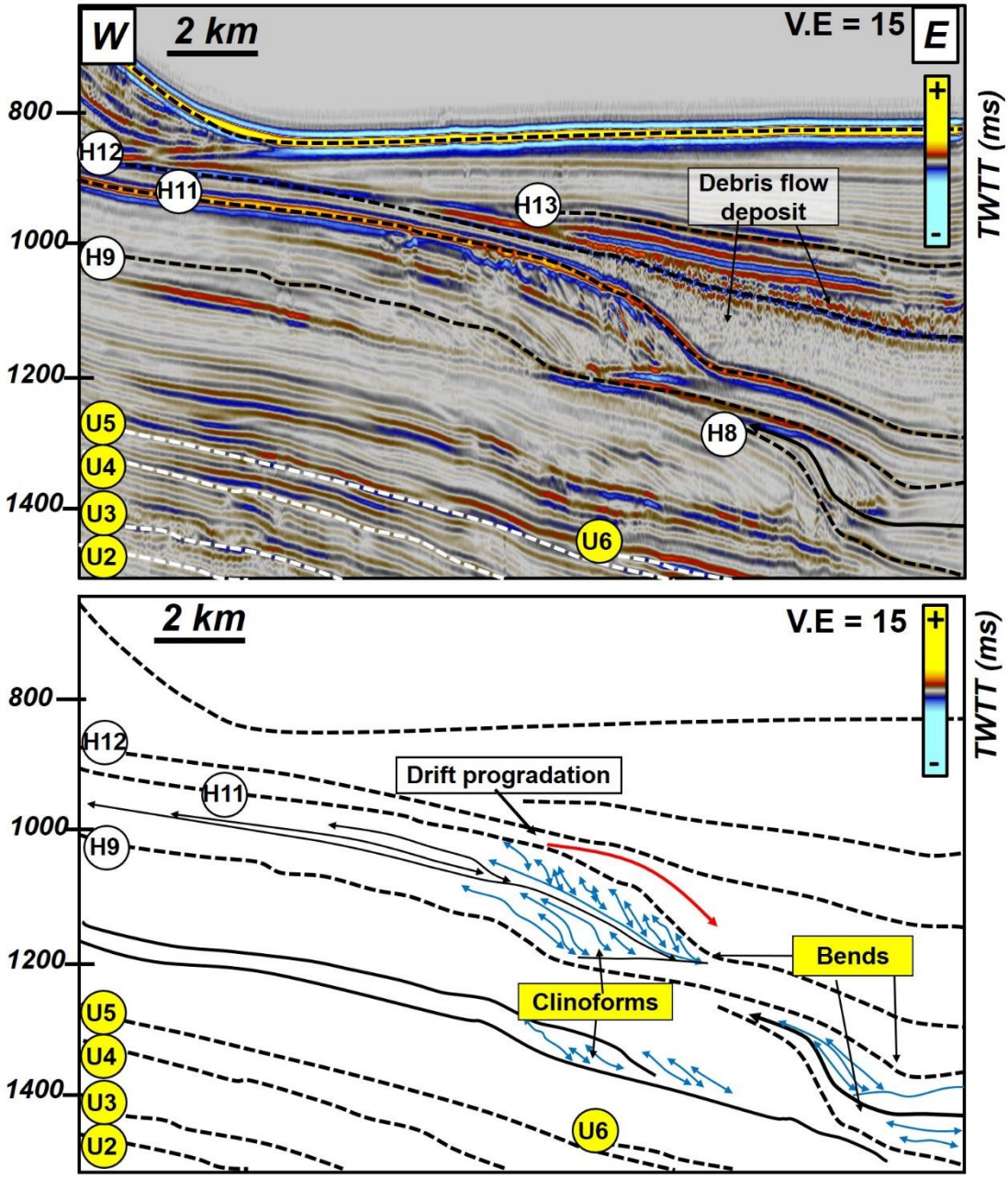
W
2 km
V.E = 15
E
800
1000
1200
1400
H12
H11
H13
H9
H8
U5
U4
U3
U2
U6
Debris flow deposit
TWTT (ms)
+
-
2 km
V.E = 15
Drift progradation
Bends
Clinoforms

Fig. 16

Table 1: Morphometric data for interpreted MTDs and contourite drifts

Deposits	**Maximum length (km)**	**Maximum Height (km)**	**Area (km^2)**	**Age**	**Orientation**
Mass transport deposits					
MTD 1	109	0.27	6058	Paleocene	NW-SE
MTD 2	88	0.24	4074	Paleocene	N-S
MTD 3	51	0.07	855	Oligocene	W-S
Contourite drifts					
Mound 1	172	1.19	1540	Mid Eocene to Late Eocene	N-S
Mound 2	172	1.16	1540	Late Eocene to Oligocene	N-S
Mound 3	202.4	1.17	2177	Late Eocene to Oligocene	N-S